Journal of Futures Markets

WILEY

RESEARCH ARTICLE

Deep Learning-Based Network Relationship Construction Method and Its Impact on Futures Risk Premiums

Chen Chuanglian[1] | Lin Huanheng[1] | Lin Yuting[2]

[1]Institute of Finance and Department of Finance, School of Economics, Jinan University, Guangzhou, China | [2]School of Economics, Guangdong University of Finance and Economics, Guangzhou, China

Correspondence: Lin Yuting (linyuting2016@aliyun.com)

Received: 25 December 2024 | **Revised:** 28 April 2025 | **Accepted:** 10 June 2025

Funding: Chen Chuanglian acknowledges the financial support from National Natural Science Foundation of China (Grant No. 72571112), the Natural Science Foundation of Guangdong (Grant No. 2024A1515012673), Technology Elite Navigation Project of Guangzhou (Grant No. 2024A04J6373), and Basic Project of Guangdong Financial Society (Grant No. JCKT202407). Lin Yuting acknowledges the financial support from National Statistical Science Plan Project (Grant No. 2025LY041).

Keywords: future volatility spillover | graph neural network | risk premium

ABSTRACT

This study proposes a deep learning framework, MIDAS–TGCN, to model the volatility spillover networks in futures markets and examines their impact on risk premiums. Traditional approaches typically rely on variance decomposition methods or VAR models, facing limitations in capturing high-dimensional nonlinear dependencies and integrating macroeconomic factors. Our framework combines mixed-data sampling (MIDAS) with Temporal Graph Convolutional Networks (TGCNs) to process high-frequency market data and low-frequency macroeconomic indicators through dual pathways, generating distinct short-term (market-driven) and long-term (macro-driven) volatility networks. The volatility network spillover effects derived through our proposed modeling framework not only capture structural responses to systemic events but also demonstrate enhanced robustness with reduced sensitivity to tail events compared with conventional approaches. Importantly, network spillover dynamics constructed via MIDAS–TGCN methodology exhibit significant explanatory power in decoding term structure risk premia in futures markets, which can be seen that the volatility network spillovers have asset pricing effects. This empirical validation aligns with emerging literature on high-frequency risk transmission while extending the analytical frontier through temporal graph convolutional architectures.

JEL Classification: G11, G14, G32

1 | Introduction

As one of the most actively traded derivatives instruments, futures contracts exhibit price discovery and risk management attributes that fundamentally depend on volatility dynamics. The intrinsic volatility–price nexus is well established in financial economics, with conventional volatility measures serving as proxies for price uncertainty (Patton and Sheppard 2015; Andersen et al. 2003). While early literature predominantly employed univariate time-series models to characterize volatility persistence (Barndorff-Nielsen and Shephard 2004; Engle et al. 2013; Chang and Yu 2013), these specifications systematically neglect cross-contract volatility interactions. Although vector autoregressive (VAR) frameworks partially address this limitation (Engle and Manganelli 2004; Reboredo and Ugolini 2020), their practical applicability diminishes rapidly with expanding the number of assets in investment portfolio due to the curse of dimensionality. Recent advances in deep learning architectures, particularly graph neural networks (GNNs) (J. Zhou et al. 2020), offer promising alternatives for

modeling high-dimensional nonlinear dependencies in multivariate volatility processes. From a theoretical perspective, both efficient market hypothesis and behavioral finance theories assume that price movements aggregate investors' heterogeneous responses to information shocks, implying that volatility dynamics embed rich informational contents including investor sentiment, risk preferences, and latent asset fundamentals. The observed nonlinearities in financial networks may reflect complex price adjustments to common market events (Ali and Hirshleifer 2020; Lee et al. 2019). These considerations motivate our dual research objectives: (1) developing deep learning methodologies to identify volatility network spillover relationships, and (2) investigating how network-implied risk factors affect futures risk premiums based on the risk-neutral pricing theory. As the world's largest commodity consumer and a pivotal node in global supply and industrial chains, and also serving as a key representative of emerging markets, the dynamics relationship of China's commodities and financial futures market have significant academic and practical value for scholarly investigation.

Volatility decomposition constitutes a critical research frontier due to its embedded informational content regarding market dynamics (Barndorff-Nielsen and Shephard 2004; Engle et al. 2013). Existing methodologies for volatility analysis are conventionally classified into two paradigms: (1) decomposition of intrinsic volatility dynamics and (2) incorporation of exogenous predictors in forecasting frameworks (Engle and Manganelli 2004; L. Wang et al. 2020; Guo et al. 2023). The literatures have established robust evidences on futures volatility determinants through both parametric and nonparametric approaches (Wei et al. 2017; Asgharian et al. 2013), with methodological implementations spanning Generalized Autoregressive Conditional Heteroskedasticity (GARCH) family models (Engle 1982), stochastic volatility frameworks (Petropoulos et al. 2022; Carverhill and Luo 2023), and heterogeneous autoregressions (Corsi 2009). Notably, recent innovations address extreme shock impacts through mixed-data sampling (MIDAS) with jump components (Guo et al. 2023), while GARCH extensions explicitly modeling tail risks demonstrate enhanced predictive accuracy (Chang and Yu 2013). Furthermore, mixed frequency data integration in multivariate time-series analysis has gained prominence, particularly through the MF-VAR model (Ghysels et al. 2016). The AI revolution has profoundly reshaped predictive modeling paradigms, with deep learning architectures demonstrating superior performance in financial forecasting tasks through hierarchical feature abstraction (Li and Yuan 2024; Salinas et al. 2020; Son et al. 2023; Yang et al. 2024). Particularly in volatility prediction and asset pricing, GNNs have emerged as transformative tools by explicitly incorporating cross-asset dependency structures—critical market signals that conventional neural architectures fail to decode effectively (Lei and Song 2024). Crucially, empirical evidence consistently identifies macroeconomic factors—particularly policy uncertainty, commodity price shocks, and inflation expectations—as exerting persistent regime-shifting effects on volatility dynamics (Wei et al. 2017; Asgharian et al. 2013).

The pervasive interdependencies among financial assets necessitate systemic risk modeling that transcends univariate volatility frameworks. Conventional single-asset specifications prove inadequate in capturing cross-asset risk spillovers, as isolated risk measures fail to characterize system-wide vulnerabilities. Network topology analysis, operationalized through graph-theoretic adjacency matrices, has emerged as the dominant paradigm for identifying systemic risk transmission mechanisms (Acemoglu et al. 2015; Diebold and Yilmaz 2009; Diebold and Yılmaz 2014; Härdle et al. 2016). Methodologically, two principal approaches dominate the estimation of directional risk linkages: Granger-causal networks and VAR-based connectedness measures (Awartani et al. 2016; Billio et al. 2012). These frameworks quantify both connection density and edge weights, with empirical studies documenting network intensification during crisis episodes (Balcilar et al. 2021; Gabauer and Gupta 2018; Lastrapes and Wiesen 2021). Significantly, incorporating network structures enhances not only systemic risk monitoring but also volatility forecasting accuracy (Foroni et al. 2015; Greenwood-Nimmo et al. 2021; Jochmann et al. 2010). Recent methodological breakthroughs integrate deep learning architectures with network topology, enabling dynamic prediction of nonlinear risk propagation patterns (Mattera and Otto 2024; Otto et al. 2024). Notably, Wu et al. (2020) pioneered an autonomous network relation learning framework that fundamentally diverges from traditional variance decomposition approaches.

The theory of storage provides the foundational framework for understanding commodity pricing dynamics, assuming that convenience yields—reflecting the implicit benefit of physical inventory holdings—exhibit positive covariation with futures risk premia (Gorton and Rouwenhorst 2006; Koijen et al. 2018; Szymanowska et al. 2014). This theoretical construct operationalizes through the basis (spot-futures spread), a widely adopted proxy for yield that demonstrates significant predictive power over global commodity returns (Boons and Prado 2019). Empirical studies further establish two critical pricing determinants: (1) Market liquidity, where elevated bid–ask spreads impede price discovery efficiency (Amihud 2002; Kang et al. 2020); and (2) Volatility dynamics, as heightened futures volatility erodes hedging effectiveness and compresses risk-adjusted returns (Bakshi et al. 2019; Menkhoff et al. 2012). Emerging research extends this paradigm by incorporating network spillover effects, with evidence confirming that cross-asset momentum transmission and risk contagion channels exert nontrivial price impacts (Y. Wang et al. 2024; Q. Zhou et al. 2023).

To the best of our knowledge, existing methodologies for measuring volatility network spillovers predominantly rely on generalized variance decomposition frameworks anchored in VAR model specifications (Diebold and Yılmaz 2014). While these approaches provide tractable solutions for computing cross-variable spillover relationships, they suffer from three critical limitations: (1) susceptibility to the curse of dimensionality, (2) sensitivity to extreme events, and (3) inability to effectively integrate macroeconomic variables into network construction (Ando et al. 2022; Ghysels 2016; Ghysels et al. 2016). Our research achieves three contributions in addressing these limitations. First, we develop a GNN framework with macro-informed node embeddings, where macroeconomic variables are systematically incorporated as nodal features through learnable representation layers. The modular neural architecture enables superior flexibility in processing mixed-frequency data compared with conventional VAR specifications. Second, while MF-VAR models enable low-frequency macro-variable integration for

high-frequency forecasting (Ghysels et al. 2016), they fundamentally lack the capability to identify the macro-driven network components within generalized variance decomposition frameworks. Our solution employs dual parallel graph networks that independently process low-frequency macroeconomic information and high-frequency market data, thereby generating distinct long-term (macro-driven) and short-term (market-driven) volatility spillover networks. Finally, although recent studies attempt to derive multihorizon networks through Fourier-based frequency-domain decomposition of VAR-estimated spillovers (Baruník and Křehlík 2018), this approach retains the persistent limitation of macro-variable integration in long-term network construction. Crucially, our novel parallel architecture resolves this through explicit separation of macro/market information flows during network learning.

Beyond methodological innovations in network construction, our research extends the analytical frontier to investigate the network-implied risk premiums in futures markets. This investigation is grounded in modern asset pricing theory, where risk-neutral pricing principles dictate that required risk compensation correlates positively with systematic risk exposures (Sharpe 1964; Lintner 1965). Unlike traditional asset-specific risk factors (e.g., liquidity, basis spreads, momentum), network relationships capture systemic interdependencies that fundamentally alter assets' risk profiles. Crucially, network centrality induces heterogeneous risk characteristics—nodes occupying strategic positions exhibit materially different risk-return profiles compared with peripheral counterparts (Lee et al. 2019; Q. Zhou et al. 2023; Ali and Hirshleifer 2020; Xu and Ye 2023; Ahern 2013). Despite this theoretical foundation, the asset pricing implications of network structures remain underexplored, primarily due to operationalization challenges in network quantification. Our study bridges this gap through two key contributions: First, we establish an analytical framework linking volatility network topology to futures risk premiums. Second, employing our novel GNN architecture, we empirically demonstrate that futures contracts occupying central network nodes command statistically significant excess risk premiums—a finding that persists across multiple robustness checks.

The structure of the paper is organized as follows: Section 2 outlines the models and metrics for network connectivity employed. Section 3 evaluates the data sets and assesses the models' predictive capabilities. Section 4 analyzes the network spillover through both static and dynamic attributes. Section 5 compares the impact of volatility network spillover derived from different measurement methods on the risk premium of futures. Finally, we make a conclusion and a summary of the findings.

2 | Model

The interdependent dynamics of asset volatilities demand rigorous quantification of cross-asset spillover effects for systemic risk assessment. Current methodological approaches predominantly employ generalized variance decomposition frameworks (Diebold and Yilmaz 2009; Diebold and Yılmaz 2014; Liu et al. 2023) to derive volatility networks through VAR specifications. However, these conventional frameworks face persistent constraints: (1) structural inability to assimilate exogenous macroeconomic information flows, and (2) methodological incapacity to isolate macro-driven long-term network components. This dual deficiency severely constrains the ability to analyze how low-frequency macroeconomic shocks transmitted through low-frequency volatility networks.

This paper proposes a novel hybrid deep learning architecture for joint modeling of volatility prediction and spillover effects. As schematically depicted in Figure 1, the proposed MIDAS–TGCN framework integrates two complementary components: (1) a temporal processing module handling mixed-frequency inputs, and (2) a relational learning module capturing cross-asset dependencies. The temporal module employs frequency-specific neural networks—separate convolutional neural networks (CNNs) process high-frequency market data and low-frequency macroeconomic indicators, respectively. The relational module combines adaptive graph learning layers with graph convolutional networks (GCNs), extending the approach of Wu et al. (2020). Specifically, our dual-graph architecture simultaneously learns short-term and long-term volatility spillover networks through parallel graph learning layers, generating dynamic adjacency matrices that quantify asset interdependencies. These graph structures then inform the spatial aggregation in subsequent GCN layers, enabling network-aware volatility estimation.

2.1 | Temporal Data Processing Module

The predominant approach for integrating deep learning algorithms with MIDAS frameworks involves constructing multiscale neural networks to analyze mixed-frequency data (Xu et al. 2023). Following this paradigm, our study employs CNNs to extract cross-frequency information. CNNs demonstrate distinct advantages in processing spatiotemporal data structures, such as those found in image and video analysis. Their architectural design enables parameter sharing through convolutional operations, which substantially reduces model complexity while mitigating overfitting risks. Through hierarchical feature learning, CNNs can automatically capture local patterns and construct high-level representations, accounting for their state-of-the-art performance in tasks ranging from image classification to speech recognition. The convolutional operation can be formalized as

$$Output_t^{\mathrm{H}} = \sigma(bias + weight \star x), \tag{1}$$

where $x = \{x_{t-1}, x_{t-2}, ..., x_{t-l}\}$ denotes the input sequence at time t, *weight* represents the parameter of the convolution kernel, and $\sigma(\cdot)$ is the sigmoid activation function. The symbol $\star$ indicates the valid convolution operator. For high-frequency data processing, we implement a hybrid architecture combining CNN and GCN layers:

$$\begin{aligned} Output_t^{\mathrm{H}} &= \sigma\left(bais_3^{\mathrm{H}} + weight_3^{\mathrm{H}} \star h_2^{\mathrm{H}}\right), \\ h_2^{\mathrm{H}} &= \mathrm{GCN}\left(\sigma\left(bais_2^{\mathrm{H}} + weight_2^{\mathrm{H}} \star h_1^{\mathrm{H}}\right), A^{\mathrm{H}}\right), \\ h_1^{\mathrm{H}} &= \mathrm{GCN}\left(\sigma\left(bais_2^{\mathrm{H}} + weight_2^{\mathrm{H}} \star x^{\mathrm{H}}\right), A^{\mathrm{H}}\right). \end{aligned} \tag{2}$$

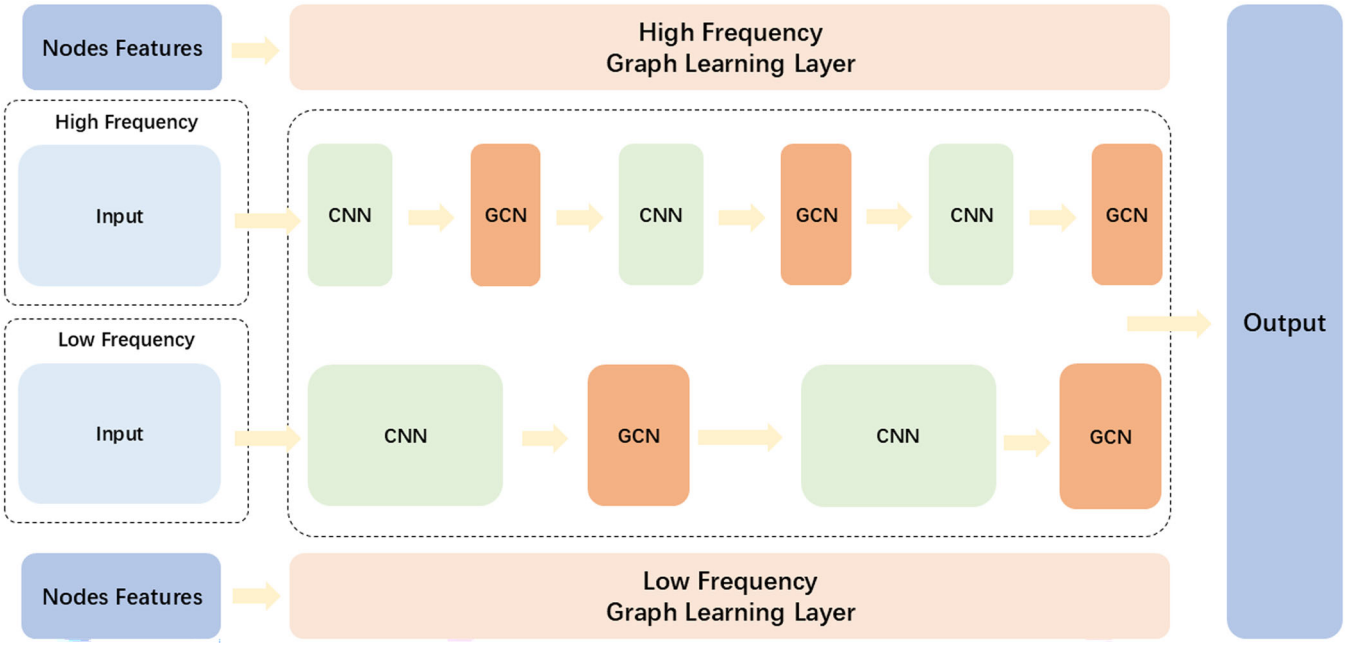

FIGURE 1 | Architectural diagram of the MIDAS–TGCN framework. CNN, convolutional neural network; GCN, graph convolutional network; MIDAS, mixed-data sampling; TGCN, Temporal Graph Convolutional Network. [Color figure can be viewed at wileyonlinelibrary.com]

Here, x^{H} corresponds to the high-frequency realized volatility (RV) series, and A^{H} encodes the adjacency matrix capturing short-term volatility spillovers among futures contracts. The low-frequency module adopts a similar structure:

$$\begin{aligned} Output_t^{\mathrm{L}} &= \sigma\left(bias_2^{\mathrm{L}} + weight_2^{\mathrm{L}} \star h_1^{\mathrm{L}}\right), \\ h_1^{\mathrm{L}} &= \mathrm{GCN}\left(\sigma\left(bias_1^{\mathrm{L}} + weight_1^{\mathrm{L}} \star x^{\mathrm{L}}\right), A^{\mathrm{L}}\right), \end{aligned} \tag{3}$$

where A^{L} characterizes long-term volatility interdependencies. A detailed description of the GCN architecture and the construction of the adjacency matrix is presented in the remaining sections.

2.2 | Network Relationship Learning Module

Volatility spillover networks play a pivotal role in enhancing forecasting accuracy and decoding cross-contract interaction mechanisms. The construction of an adjacency matrix constitutes the cornerstone of network analysis. Empirical evidence suggests that asset volatilities exhibit significant interconnectedness rather than evolving in isolation (Härdle et al. 2016). To formalize these dynamics, we establish the following mathematical framework (Balcilar et al. 2021; Bouri et al. 2018; Diebold and Yilmaz 2009):

Definition 1. (Financial network). Let $G = (V, E)$ represent a graph where $\mathbf{V}$ denotes the node set and $\mathbf{E}$ the edge set. In our context, each node $v_i \in V$ corresponds to a futures contract, while edge $e_{i,j} \in E$ quantifies the directional connectivity between contracts i and j.

Definition 2. (Spillover intensity). Let $a_{i \leftarrow j} \in [0, 1]$ $(i, j \in \{1, ..., n\})$ denote the effect of node j on node i, abbreviated as a_{ij} for notational simplicity.

Definition 3. (Adjacency matrix). weighted adjacency matrix A is defined with elements $[\mathbf{A}]_{ij} = a_{ij}$. Specifically:

- $a_{ii} = 0 \ \forall \ i$ (no self-edges),
- $a_{ij} \neq a_{ji}$ in general (asymmetric spillovers),
- $\mathbf{A}$ encodes a directed acyclic graph when it is cycle-free.

The GNN is an emerging neural network design, which was first proposed by Scarselli et al. (2008). This neural network class can process data information of graph structure; its information propagation process is shown in Figure 2. Let x_i and l_i respectively denote the state and label of the node i, $l_{(i,j)}$ represents the edge connecting nodes between i and j. e_{ij} $x_{\mathrm{ne}[i]}$ represents the set of states of nodes adjacent to node i, $l_{\mathrm{co}[i]}$ is a collection of edges with node i as an endpoint, and $l_{\mathrm{ne}[n]}$ represents the set of labels of nodes connected to point. According to Scarselli et al. (2008), there are two tasks of the GNN: node-focused and graph-focused. In this paper, GNN is used for forecasting the volatility of each futures contract; therefore, it belongs to the node-focused task. In the node-focused task, information is represented by a local transition function and a local output function. The local transition function is as follows:

$$x_i = f_w(l_i, l_{\mathrm{co}[i]}, x_{\mathrm{ne}[i]}, l_{\mathrm{ne}[i]}) \tag{4}$$

Where the w is the learnable parameters and the local output function is as follows:

$$o_i = g_w(x_i, l_i). \tag{5}$$

As shown in Figure 2, when calculating only the information of the node with which it is associated will be used for the calculation, such as the information of nodes 2, 3, 4, and 6.

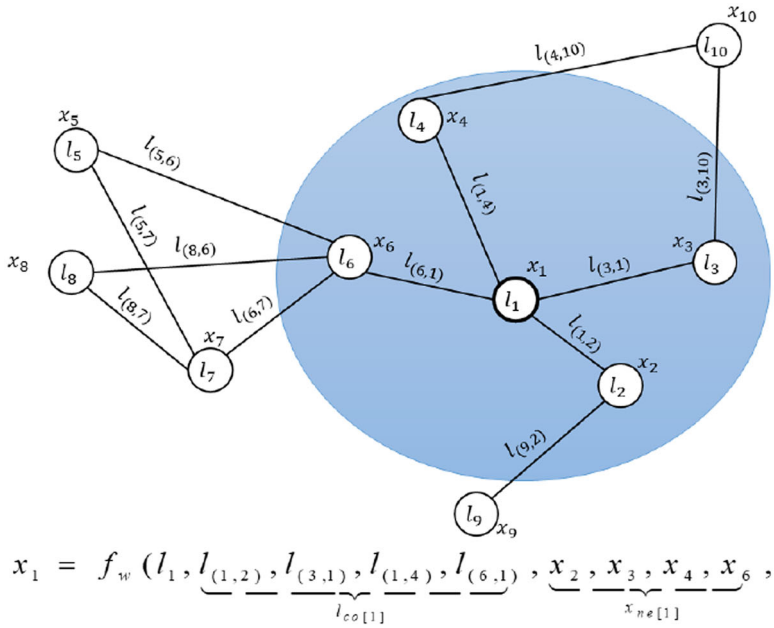

FIGURE 2 | The structure of the MIDAS–TGCN model. MIDAS, mixed-data sampling; TGCN, Temporal Graph Convolutional Network. [Color figure can be viewed at wileyonlinelibrary.com]

As discussed, traditional GNNs require predefined adjacency matrices to capture graph structural information (Wu et al. 2020). However, in financial markets, the explicit relationships between futures contracts are typically unobservable and constitute latent information that market participants seek to uncover, similar to their interest in forecasting volatility levels. To address this challenge, we adapt the graph structure learning framework proposed by Wu et al. (2020), with critical modifications to enhance numerical stability.[1]

The proposed graph learning layer is formulated as

$$M_1 = \alpha E_1 \Theta_1, \tag{6}$$

$$M_2 = \alpha E_2 \Theta_2, \tag{7}$$

$$A = \max\left(\tanh\left(\alpha\left(M_1 M_2^T - M_2 M_1^T\right)\right), 0\right). \tag{8}$$

Let $E_1, E_2 \in \mathbb{R}^{n\times d}$ denote node feature matrices, where $\Theta_1, \Theta_2 \in \mathbb{R}^{d\times h}$ are learnable parameter matrices. The slope coefficient $\alpha \in (0, 1]$ regulates the activation function's sensitivity.[2] The adjacency matrix construction differs for short-term and long-term volatility networks:

- *Short-term network:* Inputs $\left\{\mathrm{RV}_{t-k}\right\}_{k=1}^{10}$, the RV sequence.
- *Long-term network:* Combines 12-period lagged macroeconomic variables (E_1) with trainable embeddings (E_2).

Following adjacency matrix generation, the Temporal Graph Convolutional Network (TGCN) propagation mechanism extends the GCN framework (Kipf and Welling 2016) with multihop aggregation[3]:

$$\tilde{\mathcal{A}} = \tilde{\mathcal{D}}^{-1}(\mathcal{A} + I), \quad \tilde{\mathcal{D}}_{ii} = 1 + \sum_j \mathcal{A}_{ij}, \tag{9}$$

$$H^{(k)} = \tilde{\mathcal{A}}^k X, \tag{10}$$

where K controls the neighborhood depth. This formulation balances local feature preservation and global information integration (Gasteiger et al. 2018). We set $K = 1$ through grid search to prevent oversmoothing (Wu et al. 2020). The whole pattern recognition module is

$$\begin{aligned} \mathcal{A} &= \Phi(E_1, E_2; \Theta_1, \Theta_2), \\ Z &= \mathrm{GCN}(\mathcal{A}, X_{\mathrm{input}}). \end{aligned} \tag{11}$$

2.3 | Output of the Model

As illustrated in Figure 1, the MIDAS–TGCN architecture employs a multiscale decomposition framework to process high-frequency and low-frequency data streams separately. This dual-pathway design derives short-term (σ_t^{H}) and long-term (σ_t^{L}) volatility components, following the established practices in financial econometrics (Engle et al. 2013; Chen et al. 2018). The model synthesis adopts an additive fusion mechanism to preserve scale-specific dynamics:

$$\hat{\sigma}_{t+1}^2 = \mathrm{GCN}(\mathcal{A}^{\mathrm{H}}, X^{\mathrm{H}}) + \mathrm{GCN}(\mathcal{A}^{\mathrm{L}}, X^{\mathrm{L}}). \tag{12}$$

This architectural choice offers two principal advantages:

- *Parameter disentanglement:* The short-term ($\Theta^{\mathrm{H}} = \left\{\Theta_1^{\mathrm{H}}, \Theta_2^{\mathrm{H}}\right\}$) and long-term ($\Theta^{\mathrm{L}} = \left\{\Theta_1^{\mathrm{L}}, \Theta_2^{\mathrm{L}}\right\}$) graph learning parameters remain mutually orthogonal, satisfying

$$\frac{\partial \mathcal{A}^{\mathrm{H}}}{\partial \Theta^{\mathrm{L}}} = 0 \quad \text{and} \quad \frac{\partial \mathcal{A}^{\mathrm{L}}}{\partial \Theta^{\mathrm{H}}} = 0. \tag{13}$$

- *Gradient decoupling:* Backpropagation gradients flow through independent computational graphs, preventing interference between temporal scales (Goodfellow 2016).

The modular distinguishes stems from deep learning's inherent capacity for localized gradient computation (Baydin et al. 2018). As shown in Equation (13), the chain rule decomposition yields null Jacobians between nonshared parameters, ensuring the stable training of heterogeneous volatility components. Our model architecture resolves two fundamental methodological limitations in volatility network analysis: First, unlike the MF-VAR framework (Ghysels et al. 2016) that merely introduces macro variables without structural separation, our design enables explicit isolation of macro-driven spillover networks through dedicated information pathways. This critical advancement overcomes the inherent entanglement problem based on generalized variance decomposition frameworks which the macro/market effects remain conflated. Second, contrasting with frequency-domain decomposition approaches that derive multihorizon networks via Fourier transformations (Baruník and Křehlík 2018), our architecture achieves structural separation through dual-network processing of distinct information sources: (1) high-frequency market volatility shocks for short-term networks, and (2) low-frequency macroeconomic trends for long-term networks. This source-driven separation ensures theoretical consistency between network horizons and their underlying economic drivers.

3 | Variable Description and Model-Predicted Performance

3.1 | Data

In this paper, we focus on the prediction performance of our model. We obtained data on futures contracts in the Chinese market from 2017 to 2024 from the Wind database. Because commodity futures fluctuations are closely linked to manufacturing, we use Producer Price Index data to react to the price cost of manufacturing. We retained only futures contracts that have been traded in the market since 2017. We divide the samples into a training set, a validation set, and a test set to cross-check the model, and then the error converges to produce the adjacency matrix of the network.

To measure the volatility of futures contracts, we follow the approach proposed by Liu et al. (2023) to describe the volatility of futures contracts using the RV. The RV of contract i at day t is as follows:

$$\mathrm{RV}_{i,t} = \sqrt{\sum_{k=0}^{M-1} r_{i,t-k}^2}, \tag{14}$$

where $r_{i,t}$ is the logarithmic daily return of the futures contract, $r_{i,t} = \ln(P_{i,t}/P_{i,t-1})$, and M is the window size, we used a window length of 1 week, that is, $M = 5$.

3.2 | Network Connectivity Indicators

Our volatility spillover analysis is built based on the financial network econometrics framework which is proposed by Diebold and Yılmaz (2014). Let $\mathcal{A} = [a_{ij}] \in \mathbb{R}^{N\times N}$ denote the learned adjacency matrix, where a_{ij} quantifies the directional spillover intensity from node j to i. We operationalize three key network metrics:

- *Directional exposure:*

$$\mathrm{TII}_i = \sum_{j\neq i} a_{ij} \quad \text{(Total Input Intensity)}, \tag{15}$$

$$\mathrm{TOI}_i = \sum_{j\neq i} a_{ji} \quad \text{(Total Output Intensity)}. \tag{16}$$

- *Harmonic centrality (HC):*

$$\mathrm{HC}_i = \frac{1}{N-1}\frac{1}{\sum_{j\neq i} d(i,j)}, \tag{17}$$

where $d(i,j)$ is the shortest path length between nodes i and j.

- *Total network connectivity:*

$$\mathrm{TN} = \frac{1}{N(N-1)}\sum_{i=1}^{N}\sum_{j\neq i} a_{ij}. \tag{18}$$

The TII/TOI measured indexes capture the nodal relationship strength among the variables (Billio et al. 2012), while closeness centrality identifies the information flow efficiency. The normalized connectivity metric HC $\in [0, 1]$ quantifies the market-wide spillover potential (Härdle et al. 2016). For regulators, HC serves as a financial stability gauge, with HC $\to$ 1 indicating the transmission strength of systemic risk is high (Balcilar et al. 2021).

3.3 | Spot Premiums and Term Premiums

Based on the no-arbitrage framework of Szymanowska et al. (2014), we formalize premium components using the extended cost-of-carry model (Boons and Prado 2019). Let $F_t^{(n)}$ denote the n-period futures price with corresponding spot price S_t:

$$F_t^{(n)} = S_t \exp\left(y_t^{(n)} \cdot n\right), \tag{19}$$

$$y_t^{(n)} = r_t^{(n)} + u_t^{(n)} - c_t^{(n)}, \tag{20}$$

where $y_t^{(n)}$ represents the basis variable, which can be decomposed into risk-free rate $r_t^{(n)}$, storage cost $u_t^{(n)}$, and convenience yield $c_t^{(n)}$ for commodity futures. For financial futures, we impose $u_t^{(n)} \equiv 0$ following Boons and Prado (2019).

3.3.1 | Spot Premium

The expected excess spot return decomposes into

$$\mathbb{E}_t[r_{s,t+1}] \equiv \mathbb{E}_t[\Delta s_{t+1}] = \underbrace{\pi_{s,t}}_{\text{Spot Premium}} + y_t^{(1)}, \tag{21}$$

where $\pi_{s,t}$ captures compensation for spot price risk. Equation (21) implies

$$\pi_{s,t} = \mathbb{E}_t\left[r^{(1)}_{fut,t+1}\right] = \mathbb{E}_t\left[s_{t+1} - f^{(1)}_t\right]. \tag{22}$$

3.3.2 | Term Premium

The roll return from a calendar spread strategy (long first vs. short second nearby) reveals the term premium:

$$\begin{aligned}\mathbb{E}_t\left[r^{(2)}_{fut,t+1}\right] &= \mathbb{E}_t\left[f^{(1)}_{t+1} - f^{(2)}_t\right] \\ &= \pi_{s,t+1} - \pi^{(2)}_{y,t},\end{aligned} \tag{23}$$

where $\pi^{(2)}_{y,t}$ represents the second-nearby contract's term premium. This yields the premium extraction formula:

$$\pi^{(2)}_{y,t} = \mathbb{E}_t\left[r^{(1)}_{fut,t+1}\right] - \mathbb{E}_t\left[r^{(2)}_{fut,t+1}\right]. \tag{24}$$

3.4 | Model-Predicted Performance

The operational value of financial forecasting models hinges critically on their out-of-sample predictive capacity. We implement a rigorous evaluation protocol through two distinct samples: (i) early stages of the COVID-19 outbreak (2020–2021) and (ii) the period of conflict between Russia and Ukraine (2022–2023). This temporal partitioning allows for robustness testing across heterogeneous economic conditions.

The model confidence set methodology (Hansen et al. 2011) addresses a critical limitation in conventional model comparisons by endogenously determining superior forecasters without prespecified benchmarks. The procedure iteratively eliminates inferior models through pairwise loss comparisons until the remaining set satisfies

$$\mathbb{P}\left(\max_{m\in\mathcal{M}} \frac{\bar{d}_m}{\hat{\sigma}_m} \le \mathcal{Q}_{1-\alpha}\right) \ge 1-\alpha, \tag{25}$$

where $\mathcal{Q}_{1-\alpha}$ denotes the $(1-\alpha)$ quantile of the limiting distribution, $\bar{d}_m$ is the average loss differential, and $\alpha = 0.10$ is our significance threshold. Models surviving in this sequential elimination process constitute the confidence set with 90% probability. We use mean absolute error (MAE) and mean squared error (MSE) as prediction error measures.

The empirical results demonstrate that MIDAS–TGCN has superior predictive accuracy during the pandemic recovery phase, particularly based on the statistics of MAE (0.1216 vs. 0.1347 for long short-term memory [LSTM]). During monetary tightening periods, while GRU achieves marginally better MSE (0.0270), MIDAS–TGCN maintains robustness in absolute error terms (MAE, 0.1141). Traditional time-series models (AR or ARMA) exhibit systematic prediction errors exceeding 0.79 across all regimes, indicating their inadequacy in estimating the volatility of futures markets (Table 1).

4 | Volatility Network Analysis

4.1 | Static Characterization of Network Connectivity

Before we discuss the dynamics of network connectivity, we first analyze the static characteristics of network connectivity. Such static features can be regarded as unconditional features, and the analysis of these static features can be used to make a preliminary judgment about the importance of each node in the network (Diebold and Yılmaz 2014; Gong et al. 2021; Liu et al. 2023).

Table 2 presents the network analysis results, presenting the node centrality, volatility output intensity, and input intensity across different time periods. Panel A examines the short-term volatility network dynamics. In the full-sample static network, copper futures (CU.SHF) exhibits the highest total output intensity (TOI = 34.8962), while PTA (is terephthalic acid, a chemical raw material that is the main commodity futures target, short for PTA) futures (TA.CZC) shows the greatest total input intensity (TII = 20.1091). During the COVID-19 containment period (2020–2023), lead futures (PB.SHF) has the maximum volatility output intensity (TOI = 30.1454), while soybean oil futures (Y.DCE) simultaneously displays the highest volatility input strength and network centrality (HC = 0.9491). With the Russia–Ukraine conflict outbreak, manganese–silicon futures (SM.CZC) emerges as the dominant volatility output nodes, whereas palm oil futures (P.DCE) becomes the most

TABLE 1 | The MCS test results of different models.

	MIDAS–TGCN	GRU	LSTM	AR	ARMA
2020–2023					
MSE	0.0294	0.0743	0.0369	0.9981	1.0277
MAE	0.1216	0.2054	0.1347	0.7979	0.8121
2022–2023					
MSE	0.0405	0.0270	0.2684	1.0040	1.0179
MAE	0.1141	0.1497	0.4951	0.7997	0.8048

Note: This table shows the results of the out-of-sample predictions of each model, which report the prediction errors of each model for two different prediction periods. We used two error metrics, MSE and MAE, to measure the accuracy of the models' predictions. The MSE and MAE are calculated using the formulas $\text{MAE} = \sum_{i=0}^{N}|y_i - \hat{y}_i|$ and $\text{MSE} = \sum_{i=0}^{N}(y_i - \hat{y}_i)^2$, respectively. The values of these loss functions were subjected to the MCS test, and all p values greater than 0.1 were bolded.
Abbreviations: AR, autoregressive; ARMA, autoregressive moving average; GRU, gated recurrent unit; LSTM, long short-term memory; MAE, mean absolute error; MCS, model confidence set; MIDAS, mixed-data sampling; MSE, mean squared error; TGCN, Temporal Graph Convolutional Network.

TABLE 2 | The network analysis of short-term and long-term volatility networks.

	Full sample		2020–2023		2021–2022		
	Contract	Value	Contract	Value	Contract	Value	
Panel A: Short-term volatility							
Maximum							
TOI	CU.SHF	34.8962	PB.SHF	30.1454	SM.CZC	29.6932	
TII	TA.CZC	20.1091	Y.DCE	33.2188	P.DCE	20.5177	
Harmonic centrality	TA.CZC	0.5745	Y.DCE	0.9491	P.DCE	0.5862	
Panel B: Long-term volatility							
Maximum							
TOI	Y.DCE	34.8434	PP.DCE	34.9861	OI.CZC	34.7063	
TII	PP.DCE	34.4494	SN.SHF	34.9419	SN.SHF	34.8999	
Harmonic centrality	PP.DCE	0.9842	SN.SHF	0.9983	SN.SHF	0.9971	

Note: This table shows the centrality, output intensity, and input intensity of network nodes in different sample periods. Panels A and B show the results of the analysis of the short-term and long-term volatility networks, respectively. Calculations of the closeness centrality are normalized so that the HC result ranges from 0 to 1, and the higher the value, the higher the centrality of the node.
Abbreviations: HC, harmonic centrality; TII, Total Input Intensity; TOI, Total Output Intensity.

impacted nodes and network centers. Panel B analyzes the long-term volatility network characteristics. The full-sample static network reveals soybean oil futures (Y.DCE) with the highest output intensity and polypropylene futures (PP.DCE) with the maximum input intensity. From 2020 to 2023, soybean oil futures maintained their position as the network's primary output node, with tin futures (SN.SHF) attaining central network status (TII = 34.9419). This pattern persists in the 2021–2022 static network configuration.

Subsequently, we examine the attributes of high-volatility contracts across diverse networks. Figure 3 presents the characteristics of high-volatility futures contracts within short-term and long-term volatility networks for each period. The iron ore contract (I.DCE) exhibits the highest volatility throughout the sample periods. As demonstrated in panel (a), the iron ore contract (I.DCE) is more influenced within the short-term volatility network compared with the long-term volatility network. Figure 3 illustrates the characteristics of iron ore contracts in both static and dynamic networks during the COVID-19 control period. Irrespective of the short-term or long-term volatility network, the iron ore contract (I.DCE) receives greater volatility inputs, although its output strength is more pronounced in the long-term volatility network than in the short-term network. Nevertheless, this characteristic underwent a significant transformation following the Russia–Ukraine conflict. Iron ore contracts display greater volatility spillovers in the short-term volatility network and experience more volatility input from other nodes in the long-term volatility network.

4.2 | Dynamic Process of Network Connectivity

Following the static analysis of the network, this study investigates the dynamic properties of network connectivity. Employing established methodologies (Liu et al. 2023; Yarovaya et al. 2017; Gong et al. 2021; Zhang et al. 2024; Liu et al. 2023), we utilize a rolling-window approach to compute daily network adjacency matrices, thereby deriving metrics of network connectivity.

Figure 4 delineates the time-varying structural properties of volatility spillover networks across futures markets. Our MIDAS–TGCN framework captures how network connectivity responds to major economic shocks, with statistically distinguishable responses across asset classes and time horizons. First, short-term volatility networks demonstrate acute sensitivity to exogenous shocks, exemplified by the immediate connectivity surge during the COVID-19 and dramatic fluctuations during China–US trade tensions. Second, the 2021 Chinese commodity market anomalies reveal divergent temporal dynamics: short-term networks show progressive connectivity, while long-term networks maintain stable linkages. Third, the COVID-19 crisis induced persistent connectivity increases across all networks, with maximum intensity observed in financial futures' short-term spillovers. In addition, financial futures exhibits higher contagion dynamics than commodity futures.

We compare the dynamic characteristics of long- and short-term volatility spillover networks constructed by our model with those derived from traditional methods. First, we examine the sensitivity of conventional frameworks to extreme values. As shown in Figure 5, the total network connectivity based on the Diebold and Yilmaz (DY) and Barunik and Krehlik (BK) framework displays pronounced spikes during major events, which is also evident across all VAR-model-based volatility network connectivity as demonstrated in Figures 4 and 6. Notably, the long-term volatility network connectivity under the BK framework exhibits marked discontinuities, suggesting excessive sensitivity to extreme values—a critical limitation given that long-term volatility network connectivity is generally expected to maintain relative stability. The observed abrupt fluctuations contradict the theoretical premise that volatility network connectivity structures should demonstrate gradual evolutionary patterns. In contrast, the long-term volatility network connectivity derived from the MIDAS–TGCN model exhibits no abnormal fluctuations without discernible triggers. Furthermore, the model demonstrates heightened sensitivity to several major market events. As evidenced by the comparative analysis of Figures 4 and 5, the price dislocations in the futures

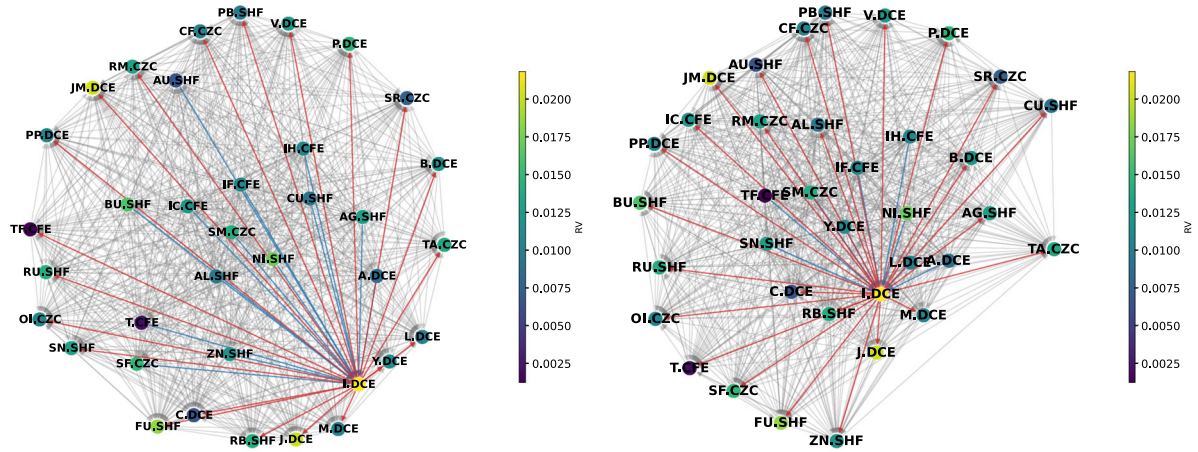

(a) Full Sample

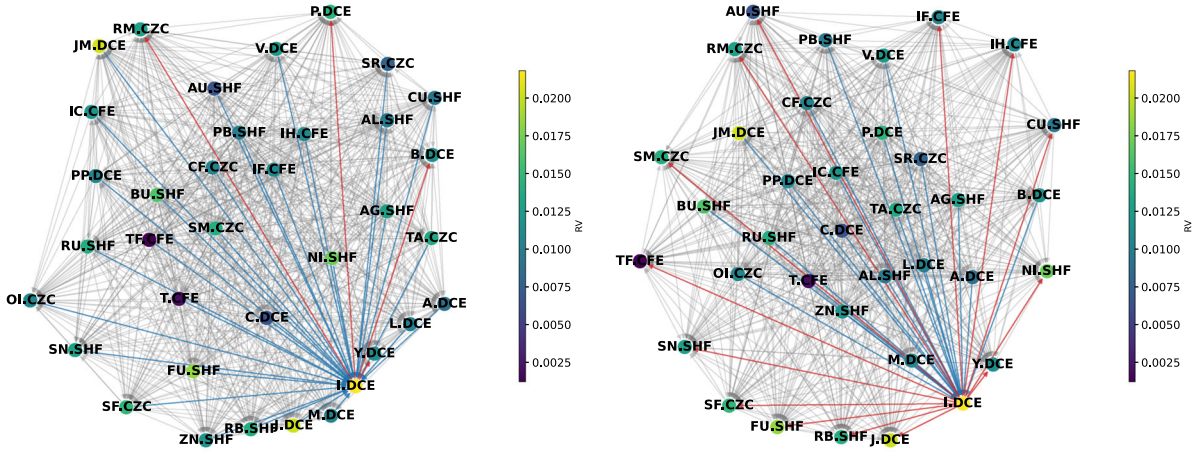

(b) 2020-2023

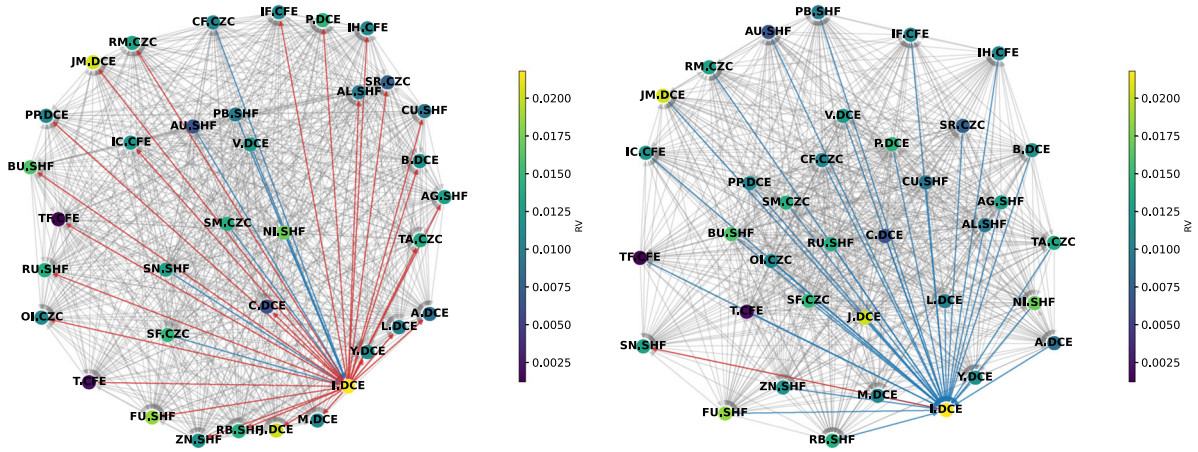

(c) 2021-2022

FIGURE 3 | Static characteristics of the network in different sample periods. The left part shows the short-term volatility network, and the right part shows the long-term volatility network. Panel (a) shows the static network characteristics during the full sample period, panel (b) shows the static network characteristics during the outbreak of COVID-19, and panel (c) shows the static network characteristics during the Russian-Ukrainian conflict. Darker nodes indicate greater realized volatility. The red line represents an overflow to other nodes, and the black line indicates input from other nodes. [Color figure can be viewed at wileyonlinelibrary.com]

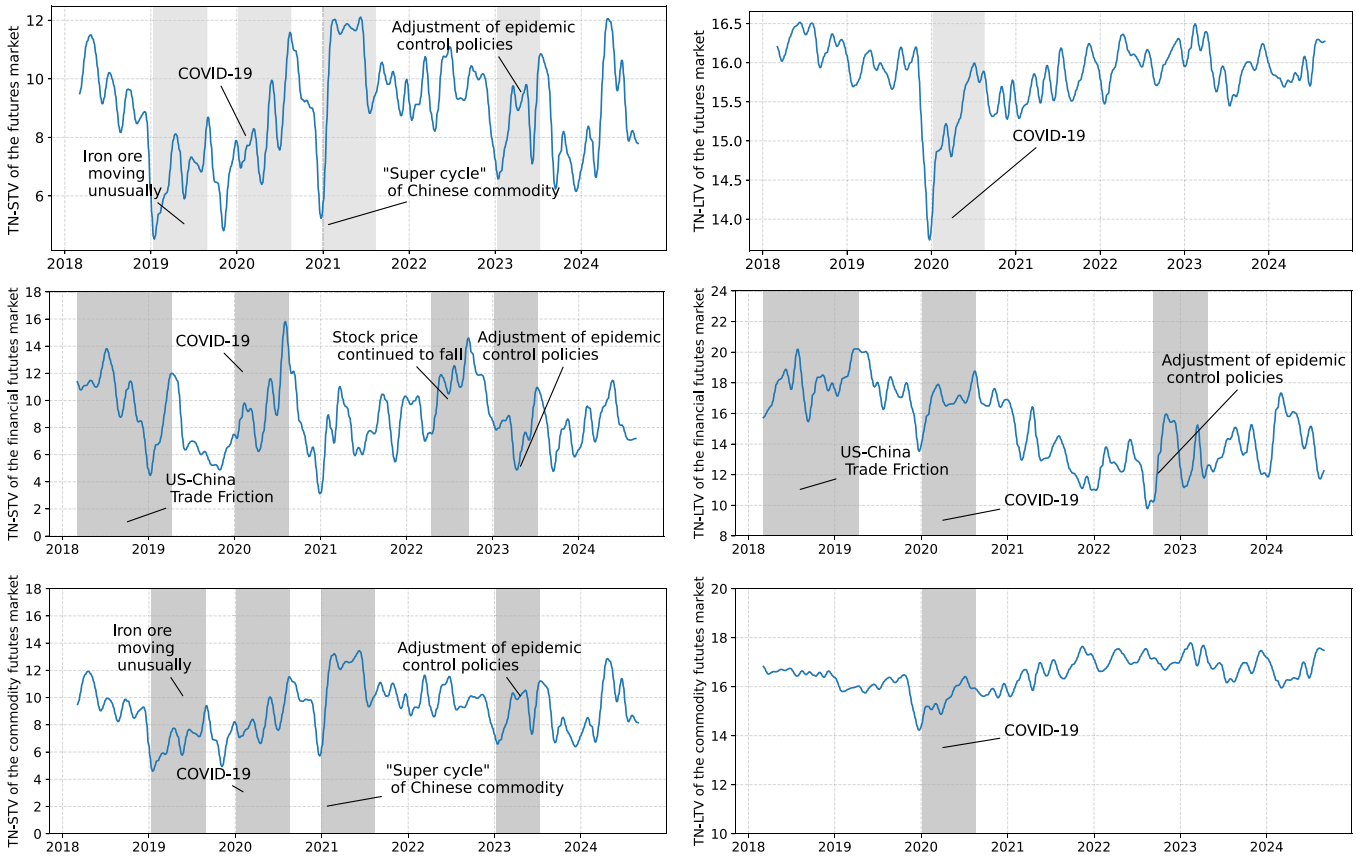

FIGURE 4 | Total network connectivity based on MIDAS–TGCN. *Note:* TN-STV denotes the total network connectivity of the short-term volatility, and TN-LTV denotes the total network connectivity of the long-term volatility. The right part denotes the short-term volatility network, and the left part denotes the long-term volatility network. MIDAS, mixed-data sampling; TGCN, Temporal Graph Convolutional Network. [Color figure can be viewed at wileyonlinelibrary.com]

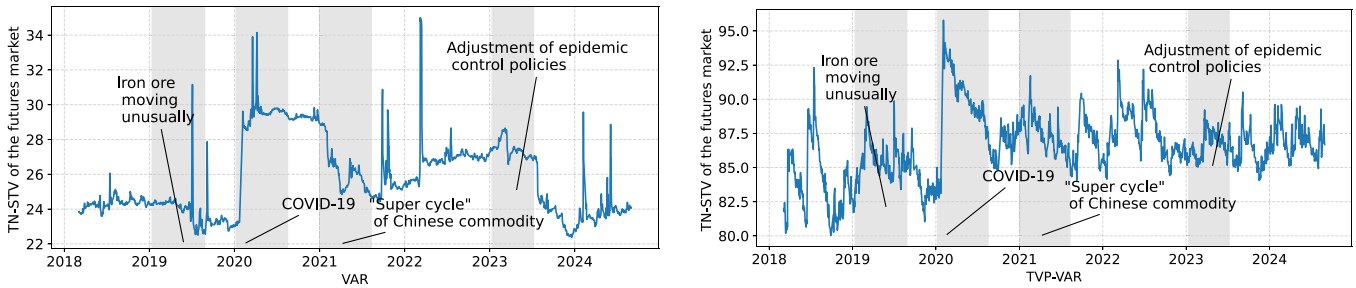

FIGURE 5 | Total network connectivity: Based on VAR and time-varying-parameter (TVP)-VAR. VAR, vector autoregressive. [Color figure can be viewed at wileyonlinelibrary.com]

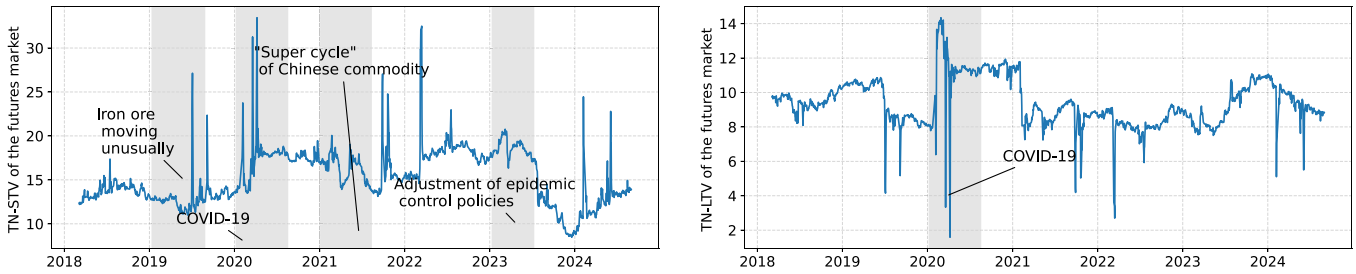

FIGURE 6 | Total network connectivity based on the BK framework. *Note:* TN-STV denotes the total network connectivity of the short-term volatility, and TN-LTV denotes the total network connectivity of the long-term volatility. The right part denotes the short-term volatility network, and the left part denotes the long-term volatility network. BK, Barunik and Krehlik. [Color figure can be viewed at wileyonlinelibrary.com]

market induced by iron ore's anomalous 2019 price movements remain undetected in the DY framework's VAR-based network. Notably, both DY (Figure 5) and BK (Figure 6) frameworks exhibit persistent declines in network connectivity as China's commodity futures market entered its 2021 "super cycle" phase. While conventional financial theory posits that abnormal asset price movements should elevate network connectivity, the DY and BK frameworks fail to adequately capture these dynamics. Conversely, the MIDAS–TGCN-based volatility network displays superior responsiveness to such structural market shifts (Figure 4).

5 | The Spillover Relationship and its Impact on the Risk Premium

This section examines the implications of volatility spillover pricing for futures contracts. We establish a comparative analytical framework between two network spillover specifications: (1) the adaptive graph learning architecture developed in our study, and (2) the exogenously defined network topology proposed by Diebold and Yılmaz (2014) and Baruník and Křehlík (2018).

5.1 | Deep Learning-Based Analysis of the Relational Pricing Power of Volatility Networks

Asset interconnectedness exerts significant influence on pricing dynamics through two primary transmission channels: (1) investor attention-driven behavioral spillovers, and (2) fundamental economic linkages. For instance, technology firms' equity valuations demonstrate mutual dependencies arising from shared technological platforms (Lee et al. 2019; Q. Zhou et al. 2023; Ali and Hirshleifer 2020). Traditional asset correlation methodologies relying on exogenous characteristics struggle to capture multidimensional interdependencies, particularly failing to identify their nonlinear interdependencies. Recent literatures demonstrate that network-implied relationships derived from sophisticated measurement frameworks significantly affect asset pricing mechanisms (Xu and Ye 2023; Y. Wang et al. 2024). This study specifically examines how volatility networks generated through our modeling approach influence futures contract risk premiums.

We then adopt our analysis by employing a portfolio approach to investigate how network relationships influence risk premia. Following Boons and Prado (2019), we classify 36 futures contracts into three portfolios (High 4, Mid, Low 4) sorted by network centrality, with each contract equally weighted in computing spot and term premia. Table 3 documents three key findings. First, the short-term volatility spillover network generates more significant portfolio returns than its long-term counterpart. Specifically, Panel A shows the low-volatility input (TII) portfolio delivering a weekly spot premium of $^{-}0.25\%$ ($t = -1.77$), with the High–Low spread portfolio yielding 0.29% weekly. In contrast, the TII-sorted portfolio exhibits no significant term premium. Second, Panel B demonstrates that the High 4 TOI portfolio based on short-term networks achieves 0.13% weekly ($t = 2.20$), with the difference portfolio generating 0.20% ($t = 2.19$). Finally, we use Diebold and Yılmaz's (2014) methodology, which reveals that their volatility spillover measure cannot construct portfolios with statistically significant premia. As evidenced in Panel C of Table 3, volatility network spillovers estimated through the VAR-based framework cannot generate portfolios with statistically significant returns. While the TVP-VAR-based approach yields portfolios demonstrating economically significant returns, these fail to exhibit significant alpha in subsequent factor model analyses, as detailed in Appendix A. Furthermore, we utilize the long- and short-term volatility spillover dynamics decomposed through the BK framework as proposed by Baruník and Křehlík (2018). Panels A and B (right-hand side) show that neither the long-term nor short-term spillover dynamics derived from this framework produce statistically significant returns.

Based on portfolio theory, we investigate whether network spillovers predict futures contract term premia to identify the ability of MIDAS–TGCN model can capture volatility spillover-driven term premia. Table 4 documents three key findings through regression analysis of term premia on contemporaneous volatility networks. First, Panel A reveals that short-term volatility spillovers significantly predict next-period term premia (0.14%). Second, Panel B demonstrates that long-term spillovers exert stronger predictive power (0.22%). Third, this network-premium relationship persists when controlling for individual fixed effects and additional covariates. The results confirm that volatility network centrality not only captures cross-sectional return differences but also contains forward-looking pricing information. Table 4 demonstrates that network spillover relationships exhibit significant predictive power for futures risk premiums. This finding naturally raises the question of whether the volatility network factor embeds informational uniqueness relative to established risk factors. Specifically, the topological structure of financial networks–a fundamental determinant of systemic risk propagation (Ali and Hirshleifer 2020; Ahern 2013; Acemoglu et al. 2015; Ramírez 2024)–endows the volatility network factor with distinct pricing signals absent in conventional risk models. Table 5 presents the Newey–West regression results, a method chosen for its robustness to heteroskedasticity and autocorrelation, thus providing more reliable standard error estimates. Panel B of Table 5 reveals that the long-term volatility spillover relationship factors do not generate significant alpha. Furthermore, these factors are largely explained by the basis factors, suggesting that the long-term volatility network relationship factor does not provide incremental factor information. Panel A in Table 5 reveals that the spillover factor for short-term volatility contains information not included in the basis factor, with $\alpha = -0.0006$ (Newey-West—h-a-c—standard error = 0.0003). This suggests that the short-term volatility spillover factor $R^{'\text{term}}_{\text{TOI}}$ contains information not explained by the basis factor.

Conventional asset pricing theories predominantly build on risk-neutral pricing frameworks. While the CAPM (Sharpe 1964) establishes the fundamental risk-return tradeoff through systematic risk exposure, it omits critical pricing components arising from cross-asset linkages (Bollerslev et al. 2018). Economic theory suggests that interasset interactions generate informational complexity that markets cannot instantaneously incorporate (Cohen and Frazzini 2008; Ozsoylev et al. 2014; Sornette 2017; Ali and

TABLE 3 | Univariate portfolio analysis.

	MIDAS–TGCN				BK			
	High 4	**Midium**	**Low 4**	**Difference**	**High 4**	**Midium**	**Low 4**	**Difference**
Panel A: Spot premium								
Short TOI	−0.0004	0.0002	0.0001	−0.0004	0.0014	0.0000	−0.0007	0.0020
	(−0.2750)	(0.2674)	(0.0469)	(−0.2342)	(0.9793)	(0.1092)	(−0.3959)	(1.1011)
Short TII	0.0004	0.0005	−0.0025*	0.0029*	0.0007	0.0000	0.0004	0.0003
	(0.2882)	(0.5945)	(−1.7708)	(1.7459)	(0.5004)	(0.0455)	(0.2915)	(0.2272)
Long TOI	0.0001	0.0001	0.0003	−0.0002	0.0001	0.0001	0.0003	−0.0002
	(0.0888)	(0.1546)	(0.3012)	(−0.1273)	(0.0705)	(0.1561)	(0.2884)	(−0.1094)
Long TII	0.0003	0.0001	0.0002	0.0001	0.0011	0.0001	−0.0004	0.0015
	(0.2804)	(0.1421)	(0.1563)	(0.0566)	(0.7847)	(0.1048)	(−0.3505)	(1.0082)
Panel B: Term premium								
Short TOI	0.0013**	0.0003	−0.0007	0.0020**	−0.0002	0.0004	0.0002	−0.0004
	(2.2014)	(1.1040)	(−1.0095)	(2.1880)	(−0.2745)	(1.5891)	(0.2937)	(−0.3950)
Short TII	−0.0003	0.0004*	0.0002	−0.0001	0.0003	0.0003	0.0001	0.0002
	(−0.4478)	(1.7556)	(−0.2821)	(−0.0835)	(0.3652)	(1.2710)	(0.3442)	(0.1623)
Long TOI	0.0011	0.0002	0.0003	0.0008	−0.0000	0.0004	0.0001	−0.0001
	(1.4886)	(0.7196)	(0.9694)	(0.9835)	(−0.0670)	(1.4341)	(0.0988)	(−0.1154)
Long TII	−0.0000	0.0002	0.0011	−0.0011	0.0003	0.0003	0.0000	0.0003
	(−0.0808)	(0.0002)	(1.4242)	(−1.3214)	(0.6012)	(1.0890)	(0.0653)	(0.3859)
Panel C: Spot and term premium								
	VAR				**TVP-VAR**			
TOI (S.P.)	0.0013	−0.0000	0.0007	0.0006	0.0011**	0.0002	−0.0014	0.0025
	(0.7496)	(−0.0268)	(0.6890)	(0.3938)	(2.1226)	(0.2758)	(−0.9170)	(1.5423)
TOI (T.P.)	0.0001	0.0002	0.0003	−0.0002	0.0005*	0.0003	0.0004	0.0002
	(0.2041)	(0.8961)	(1.0654)	(−0.2998)	(1.7319)	(0.9100)	(0.4562)	(0.1852)
TII (S.P.)	−0.0008	0.0003	0.0006	−0.0014	0.0007	0.0000	0.0004	0.0003
	(−0.5448)	(0.3097)	(0.4643)	(−0.8748)	(0.5004)	(0.0455)	(0.2915)	(0.2272)
TII (T.P.)	0.0004	0.0003	−0.0003	−0.0003	0.0004	−0.0000	−0.0004	−0.0003
	(0.7555)	(1.1810)	(−0.6385)	(−0.3870)	(1.5975)	(−0.1466)	(−0.3505)	(−0.3179)

Note: This table presents the unconditional performance in both spot premium (S.P.) (Panel A) and term premium (T.P.) (Panel B) returns of portfolios sorted on the volatility network relationship. The left part of this table shows the network relations learned based on MIDAS–TGCN, and the right part shows the network relations constructed by the generalized variance decomposition method designed by Baruník and Křehlík (2018). The Pable C shows both spot and term premium returns of portfolios sorted on the volatility network relationship which is estimated through the variance decomposition based o VAR and TVP (time-varying parameter)-VAR, respectively. For the calculation of the portfolio spot premium and term premium, we follow the approach of Boons and Prado, which states that the portfolio's spot premium is the equal-weight average return of first-nearby contracts, and the term premium is the equal-weight average of the difference between the return of first-nearby contracts and second-nearby contracts. We report the Newey–West heteroskedasticity and autocorrelation consistent (short for h.a.c.) *t* statistics in brackets. Abbreviations: BK, Barunik and Krehlik; MIDAS, mixed-data sampling; TGCN, Temporal Graph Convolutional Network; TII, Total Input Intensity; TOI, Total Output Intensity; VAR, vector autoregressive.

*, **, and *** indicate 10%, 5%, and 1% statistical significance levels, respectively.

Hirshleifer 2020), particularly given investors' limited capacity to process complex network interactions in real-time. Based on this theoretical foundation, we crucially adapt the Boons and Prado (2019) methodology through structural extensions to examine whether exposure to volatility spillover network effects commands distinct risk premia in cross-sectional asset pricing. We consider two different cross-sectional regressions. The first uses the short-term volatility spillover relationship, and the other uses the long-term volatility spillover relationship. Given the instability of a single futures contract's beta, we use a 1-year window rolling estimate to obtain the time-varying beta, following the methodology of Boons and Prado (2019). Table 6 presents the Fama–MacBeth regression results. As shown in Table 6, the short-term volatility spillover factor captures greater term risk pricing than the long-term volatility spillover factor. The short-term volatility spillover factor captures 0.17% term risk premium per week, while the long-term volatility spillover captures only −0.01% term risk premium. The term risk captured by the short-term volatility spillover factor (0.17%) is similar to the average return of the factor (0.2%). This conclusion is similar to the conclusion of Ozsoylev et al. (2014), which is that high-impact assets will have a significant premium. In addition, the short-term

TABLE 4 | Pooled regressions of the term premium on the volatility network relationship.

α	β_{TOI}	β_{TII}	β_{Basis}	β_{mom}	β_{bm}	Contract FE	*Adjusted* R^2	*Observations*
Panel A: Short-term volatility network								
−0.0019	0.0014**		0.2240***			Yes	0.00669	10,980
(0.0014)	(0.0007)		(0.0256)					
−0.0017	0.0013*		0.2417***	0.0038		Yes	0.0671	10,980
(0.0014)	(0.0007)		(0.0258)	(0.0034)				
−0.0017	0.0013*		0.2387***	0.0050	−0.0056	Yes	0.0672	10,980
(0.0014)	(0.0007)		(0.0270)	(0.0034)	(0.0090)			
−0.0017	0.0013*		0.2232***	0.0048	−0.0048	No	0.0649	10,980
(0.0014)	(0.0007)		(0.0262)	(0.0034)	(0.0088)			
−0.0012		0.0010	0.2400***			Yes	0.0667	10,980
(0.0017)		(0.0008)	(0.0256)					
−0.0010		0.0010	0.2418***	0.0040		Yes	0.0670	10,980
(0.0017)		(0.0008)	(0.0259)	(0.0034)				
−0.0010		0.0009	0.2389***	0.0052	−0.0057	Yes	0.0670	10,980
(0.0017)		(0.0008)	(0.0270)	(0.0034)	(0.0090)			
−0.0006		0.0007	0.2232***	0.0050	−0.0049	No	0.0647	10,980
(0.0017)		(0.0008)	(0.0262)	(0.0034)	(0.0088)			
Panel B: Long-term volatility network								
−0.0033	0.0016*		0.2402***			Yes	0.00668	10,980
(0.0027)	(0.0010)		(0.0256)					
−0.0035	0.0016*		0.2423***	0.0043		Yes	0.0671	10,980
(0.0027)	(0.0010)		(0.0256)	(0.0034)				
−0.0035	0.0017*		0.2392***	0.0055	−0.0059	Yes	0.0671	10,980
(0.0027)	(0.0010)		(0.0270)	(0.0034)	(0.0090)			
−0.0050**	0.0022***		0.2243***	0.0054	−0.0054	No	0.0652	10,980
(0.0021)	(0.0008)		(0.0263)	(0.0034)	(0.0088)			
0.0045		−0.0012	0.2398***			Yes	0.0067	10,980
(0.0032)		(0.0012)	(0.0256)					
0.0047		−0.0013	0.2419***	0.0042		Yes	0.0669	10,980
(0.0032)		(0.0012)	(0.0259)	(0.0034)				
0.0048		−0.0014	0.2387***	0.0055	−0.0059	Yes	0.0670	10,980
(0.0032)		(0.0012)	(0.0270)	(0.0034)	(0.0090)			
0.0070***		−0.0022**	0.2239***	0.0053	−0.0059	No	0.0651	10,980
(0.0027)		(0.0009)	(0.0263)	(0.0034)	(0.0088)			

Note: This table presents results from pooled regressions of the short-term volatility network (Panel A) and the long-term volatility network (Panel B). We used weekly data for regression. We present the estimated coefficients and the Adjusted R^2; meanwhile, we report the robust standard errors in brackets.
Abbreviations: FE, fixed effects; TII, Total Input Intensity; TOI, Total Output Intensity.
*, **, and *** indicate 10%, 5%, and 1% statistical significance levels, respectively.

volatility spillover factor is significant at the 5% level, while the long-term volatility spillover fails to capture the term risk premium significantly. In addition, neither short-term nor long-term volatility receivers (TII) factor can capture significant risk premiums. This result is consistent with the results in Table 3, and it is reasonable not to be able to capture the risk pricing because the volatility receiver relationship cannot significantly predict the risk premium for the next period.

5.2 | Robustness Test

The initial section of this paper investigates the pricing implications of volatility network spillovers. The empirical findings indicate that the short-term volatility spillover factor exhibits pricing power concerning the futures term risk premium. This conclusion is substantiated by the observation that the short-term volatility spillover factor incorporates components

TABLE 5 | The network factor versus the benchmark factor.

	α	$\beta^{spr}_{B,High\ 4}$	$\beta^{spr}_{B,Low\ 4}$	β^{nb}_{BM}	*Adjusted* R^2	*Observations*
Panel A: Short-term volatility network						
R^{spot}_{TOI}	−0.0000	0.0224	−0.0195	0.0122	0.0015	1568
	(0.0004)	(0.0462)	(0.0329)	(0.0347)		
R^{term}_{TOI}	−0.0006**	0.0138	0.0760**	−0.0032	0.0084	1568
	(0.0003)	(0.0414)	(0.0374)	(0.0315)		
R^{spot}_{TII}	0.0001	−0.0112	0.0493	0.0578	0.0085	1568
	(0.0005)	(0.0730)	(0.0470)	(0.0421)		
R^{term}_{TII}	0.0002	−0.0329	−0.0088	0.0679	0.0195	1568
	(0.0005)	(0.0717)	(0.0446)	(0.0348)		
Panel B: Long-term volatility network						
R^{spot}_{TOI}	−0.0001	0.0299	0.0741*	0.0824**	0.0220	1568
	(0.0005)	(0.0379)	(0.0425)	(0.0344)		
R^{term}_{TOI}	−0.0005	0.1238***	0.2465***	0.0401	0.1070	1568
	(0.0004)	(0.0423)	(0.0444)	(0.0260)		
R^{spot}_{TII}	−0.0001	−0.0588*	−0.0742*	−0.0745**	0.0215	1568
	(0.0005)	(0.0358)	(0.0396)	(0.0330)		
R^{term}_{TII}	0.0003	−0.1479***	−0.2379***	−0.0344	0.1054	1568
	(0.0004)	(0.0424)	(0.0430)	(0.0256)		

Note: This table presents results of spanning tests that indicate whether the volatility network relationship factors provide a significant alpha. Panel A shows the result of the short-term volatility network, and Panel B shows the result of the long-term volatility network. Following Szymanowska et al. (2014), we use four basis factors: (i) R^{nb}_{B} denotes the difference between the high and low basis returns of the first nearby contract in the investment portfolio, (ii) $R^{spr}_{B,High}$ denotes the difference between the return of first and second nearby contracts in the high basis portfolio, (iii) $R^{spr}_{B,Low}$ denotes the difference between the return of first and second nearby contracts in the low basis portfolio, and (iv) the basis–momentum nearby factor (R^{nb}_{BM}). Following Boons and Prado (2019), we regard the return on holding the first nearby contract as spot premium R^{spot}, and the difference between the returns on the first and second nearby contracts as term premium R^{term}. We report the Newey–West h.a.c. standard error in brackets.

Abbreviations: TII, Total Input Intensity; TOI, Total Output Intensity.

*, **, and *** indicate 10%, 5%, and 1% statistical significance levels, respectively.

unexplained by other factors, and factor exposures effectively capture risk pricing. To assess the robustness of this result, we conduct a series of robustness checks by substituting alternative pricing factors.

To examine the robustness of the short-term volatility spillover factor, we augment the model with two established factors from asset pricing literature: the average factor R^{nb}_{AVG} and the momentum factor R^{nb}_{mom} (Bakshi et al. 2019; Boons and Prado 2019). We systematically assess sensitivity by adjusting both the rolling training window length and the RV calculation window. Panel A of Table 7 reports factor-spanning test results, revealing that the volatility spillover factor maintains statistically significant alpha values across multiple factor combinations. Furthermore, robustness checks with modified rolling-window configurations (Panel B of Table 7) and alternative RV window sizes (Table 8) confirm that the alpha retains significance, suggesting persistent unpriced information content. To further assess robustness in terms premium prediction, we investigate the stability of network spillover exposure effects. Table 9 presents the sensitivity analyses examining alternative methodological specifications. Panel A investigates varying rolling sample sizes, while Panel B explores alternating RV window sizes. Both analyses consistently retain the statistically significant predictive capacity of the spillover relationship factor for subsequent-period term premia. Collectively, these robustness checks through rigorous specification choices underscore the stability of our core empirical findings. Notably, the network pricing performance derived from the DY and BK methodological frameworks exhibits limited robustness. These findings are systematically documented in Appendix B, providing detailed evidence supporting this conclusion.

6 | Summary

This study introduces a novel deep learning framework, MIDAS–TGCN, to model volatility spillover networks in futures markets and investigates their implications for risk premiums determinant. Addressing the limitations of traditional methods (e.g., VAR models) in handling high-dimensional dependencies and integrating macroeconomic factors, this paper proposed the architecture combines MIDAS with TGCNs to deal with this limitations. The model processes high-frequency market data and low-frequency macroeconomic indicators through dual pathways, generating distinct short-term (market-driven) and long-term (macro-driven) volatility spillover networks. Key innovations include adaptive graph learning layers that dynamically capture nonlinear interdependencies among futures contracts and modular parameter disentanglement to isolate macro/market effects.

TABLE 6 | The Fama–MacBeth regression about the future contract.

	Short-term volatility				Long-term volatility			
	R_{nb}	R_{spr}	R_{nb}	R_{spr}	R_{nb}	R_{spr}	R_{nb}	R_{spr}
γ_0	0.0002	0.0002	0.0004	0.0002	0.0002	0.0002	0.0002	0.0002
	(0.0002)	(0.0002)	(0.0012)	(0.0002)	(0.0002)	(0.0002)	(0.0002)	(0.0002)
γ_{TOI}	−0.0004	0.0017**			−0.0007	−0.0001		
	(0.0017)	(0.0008)			(0.0020)	(0.0008)		
γ_{TII}			0.0018	0.0005			−0.0006	−0.0008
			(0.0012)	(0.0025)			(0.0017)	(0.0009)
$\gamma^{\mathrm{nb}}_{\mathrm{B}}$	0.0030*	0.0029*	0.0040	0.0028	0.0047**	0.0021	0.0048**	0.0026
	(0.0017)	(0.0017)	(0.0028)	(0.0023)	(0.0019)	(0.0023)	(0.0020)	(0.0022)
$\gamma^{\mathrm{nb}}_{\mathrm{BM}}$	0.0003	0.0018*	0.0001	0.0009	0.0007	0.0014	0.0012	0.0026
	(0.0012)	(0.0010)	(0.0013)	(0.0014)	(0.0013)	(0.0009)	(0.0013)	(0.0022)
$\gamma^{\mathrm{spr}}_{\mathrm{B,High\ 4}}$	−0.0002	0.0003	0.0002	0.0002	0.0010	0.0004	0.0008	0.0016
	(0.0008)	(0.0005)	(0.0008)	(0.0008)	(0.0008)	(0.0007)	(0.0008)	(0.0010)
$\gamma^{\mathrm{spr}}_{\mathrm{B,Low\ 4}}$	−0.0006	−0.0003	−0.0008	−0.0004	−0.0004	−0.0002	−0.0007	−0.0006
	(0.0008)	(0.0011)	(0.0014)	(0.0013)	(0.0011)	(0.0012)	(0.0011)	(0.0010)
Adjusted R^2	0.2841	0.2907	0.2156	0.2806	0.2787	0.2747	0.2777	0.2787
Observations	9324	9324	9324	9324	9324	9324	9324	9324

Note: This table presents cross-sectional asset pricing tests for difference factor models for each future contract. We use a sliding window to calculate the beta value of each factor, and use a 1-year window length to calculate the weekly beta of each contract. We use basis-type factors for cross-sectional asset pricing. These factors include the basis nearby factor ($R^{\mathrm{nb}}_{\mathrm{B}}$), the spreading return of High and Low basis portfolios ($R^{\mathrm{spr}}_{\mathrm{B,High\ 4}}$ and $R^{\mathrm{spr}}_{\mathrm{B,Low\ 4}}$), and the basis–momentum nearby factor ($R^{\mathrm{nb}}_{\mathrm{BM}}$). We report on the Newey–West h.a.c. standard error in brackets.
Abbreviations: TII, Total Input Intensity; TOI, Total Output Intensity.
*, **, and *** indicate 10%, 5%, and 1% statistical significance levels, respectively.

TABLE 7 | The network factor versus other factors.

	α	β^{nb}_{Basis}	$\beta^{spr}_{Basis,High\ 4}$	$\beta^{spr}_{Basis,Low\ 4}$	β^{nb}_{AVG}	β^{nb}_{mom}	*Adjusted* R^2	*Observations*
Panel A: The scroll window size is 250								
$R^{\mathrm{term}}_{\mathrm{TOI}}$	−0.0005*	0.0014	0.0123	0.0775**			0.0083	1568
	(0.0003)	(0.0238)	(0.0450)	(0.0367)				
$R^{\mathrm{term}}_{\mathrm{TOI}}$	−0.0005*		0.0142	0.0762**	−0.0215		0.0085	1568
	(0.0003)		(0.0401)	(0.0366)	(0.0520)			
$R^{\mathrm{term}}_{\mathrm{TOI}}$	−0.0006**		0.0155	0.0761**		−0.0222	0.0102	1568
	(0.0003)		(0.0409)	(0.0364)		(0.0364)		
Panel B: The scroll window size is 125								
$R^{\mathrm{term}}_{\mathrm{TOI}}$	−0.0005*	−0.0428	0.1150*	0.1432***			0.0085	1568
	(0.0004)	(0.0336)	(0.0595)	(0.0476)				
$R^{\mathrm{term}}_{\mathrm{TOI}}$	−0.0006**		0.0907*	0.1708***	0.0775**		0.0505	1568
	(0.0003)		(0.0500)	(0.0449)	(0.0367)			

Note: This table presents results of spanning tests that indicate whether the volatility network relationship factors provide a significant alpha. Panel A shows the result of the scroll window size with 250, and Panel B shows the result of the scroll window size with 125. We used five factors for the test: (i) the return of the first nearby contract for the High-minuns-Low basis portfolio ($R^{\mathrm{nb}}_{\mathrm{Basis}}$), (ii) the difference between the return of first and second nearby contracts for high basis portfolio ($R^{\mathrm{spr}}_{\mathrm{Basis,High\ 4}}$), (iii) the difference between the return of first and second nearby contracts for low basis portfolio ($R^{\mathrm{spr}}_{\mathrm{Basis,Low\ 4}}$), (iv) the average commodity market factor ($R^{\mathrm{nb}}_{\mathrm{AVG}}$), and (v) the difference of the first nearby return between high and low momentum portfolio ($R^{\mathrm{nb}}_{\mathrm{mom}}$). Following Bakshi et al. (2019), we regard the return on holding the first nearby contract as spot premium R^{spot}, and the difference between the returns on the first and second nearby contracts as term premium R^{term}. We report the Newey–West h.a.c. standard error in brackets.
Abbreviations: TII, Total Input Intensity; TOI, Total Output Intensity.
*, **, and *** indicate 10%, 5%, and 1% statistical significance levels, respectively.

TABLE 8 | The network factor versus other factors.

	(1)	(2)	(3)	(4)	(5)	(6)
α	0.0006**	0.0006**	0.0006**	0.0007*	0.0007*	0.0007*
	(0.0003)	(0.0003)	(0.0003)	(0.0004)	(0.0004)	(0.0004)
β^{nb}_{BM}	0.0670**	0.0665**	0.0544*			
	(0.0338)	(0.0339)	(0.0297)			
β^{spr}_{BM}				0.0646*	0.0643*	0.0516
				(0.0363)	(0.0364)	(0.0321)
β^{nb}_{AVG}		0.0308			0.0379	
		(0.0566)			(0.0581)	
β^{nb}_{Mom}			0.0255			0.0301
			(0.0307)			(0.0288)
Adjusted R^2	0.0182	0.0178	0.0191	0.0175	0.0172	0.0191
Observations	1564	1564	1564	1564	1564	1564

Note: This table presents results of spanning tests that indicate whether the volatility network relationship factors provide a significant alpha. We use realized volatility with a window size of 8 in calculating the volatility network overflow relation. We report the Newey–West h.a.c. standard error in brackets.
*, **, and *** indicate 10%, 5%, and 1% statistical significance levels, respectively.

TABLE 9 | The Fama–MacBeth regression with other factors.

	γ_0	γ_{TOI}	γ^{nb}_{Basis}	γ^{nb}_{AVG}	γ^{nb}_{mom}	$\gamma^{spr}_{Basis,High\ 4}$	$\gamma^{spr}_{Basis,Low\ 4}$	***Adjusted R^2***	***Observations***
Panel A: The scroll window size is 125									
R_{spr}	0.0002*	0.0017***	0.0048*			0.0004	−0.0007	0.2949	9108
	(0.0001)	(0.0006)	(0.0025)			(0.0008)	(0.0011)		
R_{spr}	0.0001	0.0015**	0.0026	−0.0021		0.0004	0004	0.2369	9108
	(0.0002)	(0.0006)	(0.0025)	(0.0009)		(0.0006)	(0.0012)		
R_{spr}	0.0001	0.0017***	0.0051**		−0.0003	0.0010	−0.0008	0.2841	9108
	(0.0001)	(0.0007)	(0.0024)		(0.0023)	(0.0007)	(0.0011)		
Panel B: The RV computed window size is 8									
R_{spr}	0.0010*	0.0025**	0.0077***			0.0027***	−0.0004	0.1283	8424
	(0.0005)	(0.0011)	(0.0029)			(0.0008)	(0.0016)		
R_{spr}	0.0007	0.0021*	0.0089***	0.0001		0.0024***	−0.0002	0.1595	8424
	(0.0008)	(0.0012)	(0.0030)	(0.0004)		(0.0006)	(0.0016)		
R_{spr}	0.0008	0.0027**	0.0099***		−0.0024	0.0029***	−0.0013	0.1800	8424
	(0.0007)	(0.0012)	(0.0023)		(0.0022)	(0.0008)	(0.0017)		

Note: This table presents cross-sectional asset pricing tests for difference factor models for each future contract. We use a sliding window to calculate the beta value of each factor, and use a 1-year window length to calculate the weekly beta of each contract. Panel A shows the result of the scroll window size with 125, and Panel B shows the result of the RV window size with 8. We used five factors for the test: (i) the return of the first nearby contract for the High-minuns-Low basis portfolio (R^{nb}_{Basis}), (ii) the difference between the return of first and second nearby contracts for high basis portfolio ($R^{spr}_{Basis,High\ 4}$), (iii) the difference between the return of first and second nearby contracts for low basis portfolio ($R^{spr}_{Basis,Low\ 4}$), (iv) the average commodity market factor (R^{nb}_{AVG}), and (v) the difference of the first-nearby return between high and low momentum portfolio (R^{nb}_{mom}). We report on the Newey–West h.a.c. standard error in brackets.
Abbreviations: RV, realized volatility; TOI, Total Output Intensity.
*, **, and *** indicate 10%, 5%, and 1% statistical significance levels, respectively.

Empirical analysis using Chinese futures data (2017–2024) demonstrates MIDAS–TGCN's superior predictive accuracy over benchmarks (LSTM, GRU) during crises like COVID-19 and the Russia−Ukraine conflict, with lower MAE (0.1216 vs. 0.1347) and MSE (0.0294 vs. 0.0743). Network metrics—TII/TOI, HC, and Total Connectivity (TC)—reveal that copper (CU.SHF) and PTA (TA.CZC) futures dominate short-term spillovers, while soybean oil (Y.DCE) and tin (SN.SHF) exhibit macro-driven centrality. Dynamic analysis highlights heightened short-term network sensitivity to events like the COVID-19 event and trade wars, contrasting with the stability of long-term networks.

The study further establishes that volatility network topology significantly impacts futures risk premiums. Portfolios sorted by short-term network centrality yield 0.29% weekly excess return ($t = 1.75$), with central nodes (e.g., iron ore futures, I.DCE) commanding systematic risk compensation. Regression analyses confirm that short-term spillovers predict term premiums ($\beta = 0.0014, t = 2.20$), persisting after controlling for basis and momentum factors. Notably, the short-term network factor ($R^{\text{TOI}}_{\text{term}}$) generates significant alpha ($-0.0006, t = -2.00$), underscoring its unique pricing information beyond conventional risk factors. Robustness checks validate these findings across rolling windows and alternative factor specifications.

The research bridges methodological gaps in financial network analysis and offers practical insights for systemic risk monitoring and portfolio optimization. By disentangling macro/market-driven spillovers and quantifying network-implied risk premiums, the framework enhances policymakers' ability to identify contagion channels and investors' capacity to hedge cross-asset risks. Future extensions could explore real-time network adjustments for dynamic asset pricing and integrate multiasset class data to map global risk transmission pathways.

Acknowledgments

Chuanglian Chen acknowledges the financial support from National Natural Science Foundation of China (Grant No. 72571112), the Natural Science Foundation of Guangdong (Grant No. 2024A1515012673), Technology Elite Navigation Project of Guangzhou (Grant No. 2024A04J6373), and Basic Project of Guangdong Financial Society (Grant No. JCKT202407). Yuting Lin acknowledges the financial support from National Statistical Science Plan Project (Grant No. 2025LY041).

Conflicts of Interest

Chuanglian Chen reports that financial support, administrative support, article publishing charges, equipment, drugs, or supplies, statistical analysis, travel, and writing assistance were provided by Jinan University. Huanheng Lin reports that statistical analysis, travel, and writing assistance were provided by Jinan University. Yuting Lin reports that administrative support, article publishing charges, statistical analysis, and writing assistance were provided by Guangdong University of Finance & Economics. If there are other authors, they declare that they have no known competing financial interests or personal relationships that could have appeared to influence the work reported in this paper.

Data Availability Statement

The data that support the findings of this study are available from the corresponding author upon reasonable request.

Endnotes

[1] In the original formulation by Wu et al. (2020), the adjacency matrix construction uses $M_1 = \tanh(\alpha E_1 \Theta_1)$ and $M_2 = \tanh(\alpha E_2 \Theta_2)$. Our empirical analysis reveals that this formulation may lead to gradient vanishing issues when connection strength differences between nodes are small. The modified Equations (6)–(8) effectively mitigate this problem while preserving the asymmetric relationship representation.

[2] While Wu et al. (2020) fix $\alpha = 3$, our analysis shows $\lim_{\alpha \to \infty} a_{ij} \to 1 \ \forall \ i, j$, causing gradient vanishing. Restricting $\alpha \in (0, 1]$ enhances numerical stability while preserving nonlinear relationships.

[3] To ensure the adjacency matrix fully captures volatility spillover relationships, we deliberately deviate from the architectural paradigm in GCNs proposed by Wu et al. (2020). Specifically, we abstain from implementing the multilayer aggregation mechanism: $Z = \sum_{k=0}^{K} H^{(k)} W^{(k)}, W^{(k)} \in \mathbb{R}^{d \times o}$.

References

Acemoglu, D., A. Ozdaglar, and A. Tahbaz-Salehi. 2015. "Systemic Risk and Stability in Financial Networks." *American Economic Review* 105, no. 2: 564–608.

Ahern, K. R. 2013. "Network Centrality and the Cross Section of Stock Returns." Available at SSRN 2197370. https://papers.ssrn.com/sol3/papers.cfm?abstract_id=2197370.

Ali, U., and D. Hirshleifer. 2020. "Shared Analyst Coverage: Unifying Momentum Spillover Effects." *Journal of Financial Economics* 136, no. 3: 649–675.

Amihud, Y. 2002. "Illiquidity and Stock Returns: Cross-Section and Time-Series Effects." *Journal of Financial Markets* 5, no. 1: 31–56.

Andersen, T. G., T. Bollerslev, F. X. Diebold, and P. Labys. 2003. "Modeling and Forecasting Realized Volatility." *Econometrica* 71, no. 2: 579–625.

Ando, T., M. Greenwood-Nimmo, and Y. Shin. 2022. "Quantile Connectedness: Modeling Tail Behavior in the Topology of Financial Networks." *Management Science* 68, no. 4: 2401–2431.

Asgharian, H., A. J. Hou, and F. Javed. 2013. "The Importance of the Macroeconomic Variables in Forecasting Stock Return Variance: A GARCH–MIDAS Approach." *Journal of Forecasting* 32, no. 7: 600–612.

Awartani, B., M. Aktham, and G. Cherif. 2016. "The Connectedness Between Crude Oil and Financial Markets: Evidence From Implied Volatility Indices." *Journal of Commodity Markets* 4, no. 1: 56–69.

Bakshi, G., X. Gao, and A. G. Rossi. 2019. "Understanding the Sources of Risk Underlying the Cross Section of Commodity Returns." *Management Science* 65, no. 2: 619–641.

Balcilar, M., D. Gabauer, and Z. Umar. 2021. "Crude Oil Futures Contracts and Commodity Markets: New Evidence From a TVP-VAR Extended Joint Connectedness Approach." *Resources Policy* 73: 102219.

Barndorff-Nielsen, O. E., and N. Shephard. 2004. "Power and Bipower Variation With Stochastic Volatility and Jumps." *Journal of Financial Econometrics* 2, no. 1: 1–37.

Baruník, J., and T. Křehlík. 2018. "Measuring the Frequency Dynamics of Financial Connectedness and Systemic Risk." *Journal of Financial Econometrics* 16, no. 2: 271–296.

Baydin, A. G., B. A. Pearlmutter, A. A. Radul, and J. M. Siskind. 2018. "Automatic Differentiation in Machine Learning: A Survey." *Journal of Machine Learning Research* 18, no. 153: 1–43.

Billio, M., M. Getmansky, A. W. Lo, and L. Pelizzon. 2012. "Econometric Measures of Connectedness and Systemic Risk in the Finance and Insurance Sectors." *Journal of Financial Economics* 104, no. 3: 535–559.

Bollerslev, T., B. Hood, J. Huss, and L. H. Pedersen. 2018. "Risk Everywhere: Modeling and Managing Volatility." *Review of Financial Studies* 31, no. 7: 2729–2773.

Boons, M., and M. P. Prado. 2019. "Basis–Momentum." *Journal of Finance* 74, no. 1: 239–279.

Bouri, E., R. Gupta, S. Hosseini, and C. K. M. Lau. 2018. "Does Global Fear Predict Fear in Brics Stock Markets? Evidence From a Bayesian Graphical Structural VAR Model." *Emerging Markets Review* 34: 124–142.

Carverhill, A., and D. Luo. 2023. "A Bayesian Analysis of Time-Varying Jump Risk in S&P 500 Returns and Options." *Journal of Financial Markets* 64: 100786.

Chang, K.-L., and S.-T. Yu. 2013. "Does Crude Oil Price Play an Important Role in Explaining Stock Return Behavior?" *Energy Economics* 39: 159–168.

Chen, X. B., J. Gao, D. Li, and P. Silvapulle. 2018. "Nonparametric Estimation and Forecasting for Time-Varying Coefficient Realized Volatility Models." *Journal of Business & Economic Statistics* 36, no. 1: 88–100.

Cohen, L., and A. Frazzini. 2008. "Economic Links and Predictable Returns." *Journal of Finance* 63, no. 4: 1977–2011.

Corsi, F. 2009. "A Simple Approximate Long-Memory Model of Realized Volatility." *Journal of Financial Econometrics* 7, no. 2: 174–196.

Diebold, F. X., and K. Yilmaz. 2009. "Measuring Financial Asset Return and Volatility Spillovers, With Application to Global Equity Markets." *Economic Journal* 119, no. 534: 158–171.

Diebold, F. X., and K. Yılmaz. 2014. "On the Network Topology of Variance Decompositions: Measuring the Connectedness of Financial Firms." *Journal of Econometrics* 182, no. 1: 119–134.

Engle, R. F. 1982. "Autoregressive Conditional Heteroscedasticity With Estimates of the Variance of United Kingrom Inflation." *Econometrica* 50: 391–407.

Engle, R. F., E. Ghysels, and B. Sohn. 2013. "Stock Market Volatility and Macroeconomic Fundamentals." *Review of Economics and Statistics* 95, no. 3: 776–797.

Engle, R. F., and S. Manganelli. 2004. "CAViaR: Conditional Autoregressive Value at Risk by Regression Quantiles." *Journal of Business & Economic Statistics* 22, no. 4: 367–381.

Foroni, C., P. Guérin, and M. Marcellino. 2015. "Markov-Switching Mixed-Frequency VAR Models." *International Journal of Forecasting* 31, no. 3: 692–711.

Gabauer, D., and R. Gupta. 2018. "On the Transmission Mechanism of Country-Specific and International Economic Uncertainty Spillovers: Evidence From a TVP-VAR Connectedness Decomposition Approach." *Economics Letters* 171: 63–71.

Gasteiger, J., A. Bojchevski, and S. Günnemann. 2018. "Predict Then Propagate: Graph Neural Networks Meet Personalized Pagerank." arXiv preprint arXiv:1810.05997. https://arxiv.org/abs/1810.05997.

Ghysels, E. 2016. "Macroeconomics and the Reality of Mixed Frequency Data." *Journal of Econometrics* 193, no. 2: 294–314.

Ghysels, E., J. B. Hill, and K. Motegi. 2016. "Testing for Granger Causality With Mixed Frequency Data." *Journal of Econometrics* 192, no. 1: 207–230.

Gong, X., Y. Liu, and X. Wang. 2021. "Dynamic Volatility Spillovers Across Oil and Natural Gas Futures Markets Based on a Time-Varying Spillover Method." *International Review of Financial Analysis* 76: 101790.

Goodfellow, I. 2016. *Deep Learning* (Vol. 196). MIT Press.

Gorton, G., and K. G. Rouwenhorst. 2006. "Facts and Fantasies About Commodity Futures." *Financial Analysts Journal* 62, no. 2: 47–68.

Greenwood-Nimmo, M., V. H. Nguyen, and Y. Shin. 2021. "Measuring the Connectedness of the Global Economy." *International Journal of Forecasting* 37, no. 2: 899–919.

Guo, Y., P. Li, and H. Wu. 2023. "Jumps in the Chinese Crude Oil Futures Volatility Forecasting: New Evidence." *Energy Economics* 126: 106955.

Hansen, P. R., A. Lunde, and J. M. Nason. 2011. "The Model Confidence Set." *Econometrica* 79, no. 2: 453–497.

Härdle, W. K., W. Wang, and L. Yu. 2016. "TENET: Tail-Event Driven NETwork Risk." *Journal of Econometrics* 192, no. 2: 499–513.

Jochmann, M., G. Koop, and R. W. Strachan. 2010. "Bayesian Forecasting Using Stochastic Search Variable Selection in a VAR Subject to Breaks." *International Journal of Forecasting* 26, no. 2: 326–347.

Kang, W., K. G. Rouwenhorst, and K. Tang. 2020. "A Tale of Two Premiums: The Role of Hedgers and Speculators in Commodity Futures Markets." *Journal of Finance* 75, no. 1: 377–417.

Kipf, T. N., and M. Welling. 2016. "Semi-Supervised Classification With Graph Convolutional Networks." arXiv preprint arXiv:1609.02907. https://arxiv.org/abs/1609.02907.

Koijen, R. S., T. J. Moskowitz, L. H. Pedersen, and E. B. Vrugt. 2018. "Carry." *Journal of Financial Economics* 127, no. 2: 197–225.

Lastrapes, W. D., and T. F. Wiesen. 2021. "The Joint Spillover Index." *Economic Modelling* 94: 681–691.

Lee, C. M., S. T. Sun, R. Wang, and R. Zhang. 2019. "Technological Links and Predictable Returns." *Journal of Financial Economics* 132, no. 3: 76–96.

Lei, B., and Y. Song. 2024. "Volatility Forecasting for Stock Market Incorporating Media Reports, Investors' Sentiment, and Attention Based on MTGNN Model." *Journal of Forecasting* 43, no. 5: 1706–1730.

Li, X., and J. Yuan. 2024. "DeepTVAR: Deep Learning for a Time-Varying VAR Model With Extension to Integrated VAR." *International Journal of Forecasting* 40, no. 3: 1123–1133.

Lintner, J. 1965. "The Valuation of Risk Assets and the Selection of Risky Investments in Stock Portfolios and Capital Budgets." *Review of Economics and Statistics* 47, no. 1: 13–37.

Liu, Z., Q. Ji, P. Zhai, and Z. Ding. 2023. "Asymmetric and Time-Frequency Volatility Connectedness Between China and International Crude Oil Markets With Portfolio Implications." *Research in International Business and Finance* 66: 102039.

Mattera, R., and P. Otto. 2024. "Network Log-ARCH Models for Forecasting Stock Market Volatility." *International Journal of Forecasting* 40, no.4: 1539–1555.

Menkhoff, L., L. Sarno, M. Schmeling, and A. Schrimpf. 2012. "Carry Trades and Global Foreign Exchange Volatility." *Journal of Finance* 67, no. 2: 681–718.

Otto, P., O. Doğan, and S. Taşpınar. 2024. "Dynamic Spatiotemporal ARCH Models." *Spatial Economic Analysis* 19, no. 2: 250–271.

Ozsoylev, H. N., J. Walden, M. D. Yavuz, and R. Bildik. 2014. "Investor Networks in the Stock Market." *Review of Financial Studies* 27, no. 5: 1323–1366.

Patton, A. J., and K. Sheppard. 2015. "Good Volatility, Bad Volatility: Signed Jumps and the Persistence of Volatility." *Review of Economics and Statistics* 97, no. 3: 683–697.

Petropoulos, F., D. Apiletti, V. Assimakopoulos, et al. 2022. "Forecasting: Theory and Practice." *International Journal of Forecasting* 38, no. 3: 705–871.

Ramírez, C. A. 2024. "Firm Networks and Asset Returns." *Review of Financial Studies* 37, no. 10: 3050–3091.

Reboredo, J. C., and A. Ugolini. 2020. "Price Connectedness Between Green Bond and Financial Markets." *Economic Modelling* 88: 25–38.

Salinas, D., V. Flunkert, J. Gasthaus, and T. Januschowski. 2020. "Deepar: Probabilistic Forecasting With Autoregressive Recurrent Networks." *International Journal of Forecasting* 36, no. 3: 1181–1191.

Scarselli, F., M. Gori, A. C. Tsoi, M. Hagenbuchner, and G. Monfardini. 2008. "The Graph Neural Network Model." *IEEE Transactions on Neural Networks* 20, no. 1: 61–80.

Sharpe, W. F. 1964. "Capital Asset Prices: A Theory of Market Equilibrium Under Conditions of Risk." *Journal of Finance* 19, no. 3: 425–442.

Son, B., Y. Lee, S. Park, and J. Lee. 2023. "Forecasting Global Stock Market Volatility: The Impact of Volatility Spillover Index in Spatial-Temporal Graph-Based Model." *Journal of Forecasting* 42, no. 7: 1539–1559.

Sornette, D. 2017. "Why Stock Markets Crash: Critical Events in Complex Financial Systems." In *Why Stock Markets Crash*. Princeton University Press.

Szymanowska, M., F. De Roon, T. Nijman, and R. Van Den Goorbergh. 2014. "An Anatomy of Commodity Futures Risk Premia." *Journal of Finance* 69, no. 1: 453–482.

Wang, L., F. Ma, J. Liu, and L. Yang. 2020. "Forecasting Stock Price Volatility: New Evidence From the GARCH–MIDAS Model." *International Journal of Forecasting* 36, no. 2: 684–694.

Wang, Y., J. Zhao, Q. Li, and X. Wei. 2024. "Considering Momentum Spillover Effects via Graph Neural Network in Option Pricing." *Journal of Futures Markets* 44, no. 6: 1069–1094.

Wei, Y., J. Liu, X. Lai, and Y. Hu. 2017. "Which Determinant Is the Most Informative in Forecasting Crude Oil Market Volatility: Fundamental, Speculation, or Uncertainty?" *Energy Economics* 68: 141–150.

Wu, Z., S. Pan, G. Long, J. Jiang, X. Chang, and C. Zhang. 2020. "Connecting the Dots: Multivariate Time Series Forecasting With Graph Neural Networks." In *Proceedings of the 26th ACM SIGKDD International Conference on Knowledge Discovery & Data Mining*, 753–763.

Xu, Q., and Y. Ye. 2023. "Commodity Network and Predictable Returns." *Journal of Futures Markets* 43, no. 10: 1423–1449.

Xu, Q., Z. Wang, C. Jiang, and Y. Liu. 2023. "Deep Learning on Mixed Frequency Data." *Journal of Forecasting* 42, no. 8: 2099–2120.

Yang, K., N. Hu, and F. Tian. 2024. "Forecasting Crude Oil Volatility Using the Deep Learning-Based Hybrid Models With Common Factors." *Journal of Futures Markets* 44, no. 8: 1429–1446.

Yarovaya, L., J. Brzeszczyński, and C. K. M. Lau. 2017. "Asymmetry in Spillover Effects: Evidence for International Stock Index Futures Markets." *International Review of Financial Analysis* 53: 94–111.

Zhang, Y., Q. Ji, D. Zhang, and K. Guo. 2024. "How Does Shanghai Crude Oil Futures Affect Top Global Oil Companies: The Role of Multi-Uncertainties." *Energy Economics* 131: 107354.

Zhou, J., G. Cui, S. Hu, et al. 2020. "Graph Neural Networks: A Review of Methods and Applications." *AI Open* 1: 57–81.

Zhou, Q., P. Zhu, and Y. Zhang. 2023. "Contagion Spillover From Bitcoin to Carbon Futures Pricing: Perspective From Investor Attention." *Energies* 16, no. 2: 929.

Appendix A

Factorial test and FM regression about other network factors

See Tables A1 and A2.

TABLE A1 | The other network factor versus the benchmark factor.

	(1)	(2)	(3)	(4)	(5)	(6)	(7)	(8)
α	0.0005	−0.0002	−0.0001	0.0004	−0.0002	0.0001	−0.0001	0.0000
	(0.0003)	(0.0004)	(0.0003)	(0.0004)	(0.0004)	(0.0003)	(0.0003)	(0.0003)
$\beta^{spr}_{B,High\ 4}$	0.1028*	0.0331	−0.1583***	0.2466***	−0.0224	0.0823**	0.0663	0.0750**
	(0.0422)	(0.0493)	(0.0500)	(0.0543)	(0.0472)	(0.0400)	(0.0430)	(0.0381)
$\beta^{spr}_{B,Low\ 4}$	0.0134	0.0644**	−0.1419***	0.2093***	0.0153	0.0685*	0.0750**	0.0552
	(0.0297)	(0.0326)	(0.0329)	(0.0387)	(0.0454)	(0.0372)	(0.0298)	(0.0350)
β^{spr}_{AVG}	−0.1418***	0.1005*	−0.0725	0.0920	0.1191	0.1063	−0.0401	0.0660
	(0.0496)	(0.0583)	(0.0541)	(0.0720)	(0.0767)	(0.0690)	(0.0544)	(0.0516)
Adjusted R^2	0.0209	0.0104	0.0640	0.1214	0.0025	0.0158	0.0133	0.0140
Observations	1348	1348	1568	1568	1568	1568	1568	1568

Note: This table presents results of spanning tests that indicate whether the volatility network relationship factors provide a significant alpha. (1) and (2) are the TOI and TII calculated using the DY framework. (3) and (4) are the TOI and TII calculated using the TVP-VAR-based DY framework. (5) and (6) are the short-term TOI and TII calculated using the BK framework. (6) and (7) are the long-term TOI and TII calculated using the BK framework.
Abbreviations: BK, Barunik and Krehlik; DY, Diebold and Yilmaz; TII, Total Input Intensity; TOI, Total Output Intensity; VAR, vector autoregressive.
*, **, and *** indicate 10%, 5%, and 1% statistical significance levels, respectively.

TABLE A2 | The Fama–MacBeth regression about the future contract.

	(1)	(2)	(3)	(4)	(5)	(6)	(7)	(8)
γ_0	0.0004	0.0003	0.0003***	0.0001	0.0004	0.0004	0.0005	0.0004
	(0.0010)	(0.0010)	(0.0001)	(0.0001)	(0.0010)	(0.0010)	(0.0011)	(0.0010)
γ^{spr}_{TOI}	−0.0006		0.0008		−0.0016		0.0020	
	(0.0011)		(0.0013)		(0.0015)		(0.0011)	
γ^{spr}_{TII}		0.0018*		0.0005		−0.0003		0.0002
		(0.0010)		(0.0010)		(0.0010)		(0.0019)
$\gamma^{spr}_{B,High\ 4}$	−0.0014	−0.0010	−0.0001	0.0009	−0.0010	−0.0008	−0.0010	−0.0004
	(0.0014)	(0.0010)	(0.0005)	(0.0007)	(0.0010)	(0.0009)	(0.0012)	(0.0016)
$\gamma^{spr}_{B,Low\ 4}$	−0.0008	−0.0019	−0.0007	−0.0006	−0.0014	−0.0013	−0.0023	−0.0023
	(0.0017)	(0.0022)	(0.0010)	(0.0011)	(0.0017)	(0.0019)	(0.0019)	(0.0022)
γ^{nb}_{B}	0.0001	0.0024	0.0017	0.0022	0.0025	−0.0009	0.0031	0.0011
	(0.0025)	(0.0033)	(0.0020)	(0.0019)	(0.0032)	(0.0023)	(0.0034)	(0.0025)
Adjusted R^2	0.1523	0.1476	0.2518	0.2582	0.1351	0.1367	0.1560	0.1400
Observations	9324	9324	9324	9324	9324	9324	9324	9324

Note: This table presents cross-sectional asset pricing tests for difference factor models for each future contract. We use a sliding window to calculate the beta value of each factor, and use a 1-year window length to calculate the weekly beta of each contract. (1) and (2) are the TOI and TII calculated using the DY framework. (3) and (4) are the TOI and TII calculated using the TVP-VAR-based DY framework. (5) and (6) are the short-term TOI and TII calculated using the BK framework. (6) and (7) are the long-term TOI and TII calculated using the BK framework. We report on the Newey–West h.a.c. standard error in brackets.

Abbreviations: BK, Barunik and Krehlik; DY, Diebold and Yilmaz; TII, Total Input Intensity; TOI, Total Output Intensity; VAR, vector autoregressive.

*, **, and *** indicate 10%, 5%, and 1% statistical significance levels, respectively.

Appendix B

Robustness test about other factors

See Tables B1 and B2.

TABLE B1 | The network factor versus other factors.

	α	$\beta^{spr}_{Beta,High\ 4}$	$\beta^{spr}_{Beta,Low\ 4}$	β^{nb}_{AVG}	*Adjusted* R^2	*Observations*
Panel A: The scroll window size is 125, and the predicted step size is 12						
TOI DY	0.0002	0.0744*	0.0857**	−0.1062	0.0245	1568
	(0.0003)	(0.0448)	(0.0413)	(0.0924)		
TII DY	−0.0000	0.0060	0.0089	0.0934	0.0008	1568
	(0.0004)	(0.0478)	(0.0422)	(0.0670)		
Short TOI BK	0.0002	−0.0331	−0.0383	0.0678	0.0033	1568
	(0.0003)	(0.0371)	(0.0294)	(0.0648)		
Short TII BK	−0.0006	−0.1001	0.0006	−0.0647	0.0125	1568
	(0.0005)	(0.0702)	(0.0346)	(0.0609)		
Long TOI BK	−0.0001	0.0514	0.0658	−0.0757	0.0105	1568
	(0.0003)	(0.0313)	(0.0415)	(0.0714)		
Long TII BK	−0.0000	0.0750**	0.0552	0.0660	0.0140	1568
	(0.0003)	(0.0381)	(0.0350)	(0.0516)		
Panel B: The scroll window size is 250, and the predicted step size is 20						
TOI DY	−0.0001	0.0895***	0.1036***	−0.1037*	0.0373	1568
	(0.0003)	(0.0344)	(0.0318)	(0.0615)		
TII DY	−0.0001	0.0664	0.0912***	0.0869	0.0205	1568
	(0.0003)	(0.0474)	(0.0347)	(0.0623)		
Short TOI BK	−0.0001	−0.0449	−0.0351	0.1071	0.0054	1568
	(0.0003)	(0.0406)	(0.0468)	(0.0797)		
Short TII BK	0.0002	0.0336	0.0032	0.0972	0.0021	1568
	(0.0004)	(0.0411)	(0.0498)	(0.0844)		
Long TOI BK	−0.0003	0.0568	0.0980***	0.1071	0.0054	1568
	(0.0003)	(0.0418)	(0.0323)	(0.0797)		
Long TII BK	0.0004	0.1057**	0.0255	0.0500	0.0157	1568
	(0.0003)	(0.0480)	(0.0297)	(0.0509)		
Panel C: The TVP-VAR predicted step size is 12						
TOI TVP-VAR	−0.0003	−0.1550***	−0.1182***	−0.0190	0.0522	1568
	(0.0003)	(0.0437)	(0.0316)	(0.0540)		
TOI TVP-VAR	0.0004	0.2455***	0.2080***	0.0966	0.1164	1568
	(0.0004)	(0.0568)	(0.0428)	(0.0836)		

Note: This table presents robustness test results of spanning tests that indicate whether the volatility network relationship factors provide a significant alpha. Panel A shows the result of spanning tests about the scroll window size of 125 and the predicted step size of 12. Panel B shows the result of spanning tests about the scroll window size of 250 and the predicted step size of 20. Panel C shows the result of spanning tests about TOI and TII computed using the TVP-VAR-based DY framework. We report on the Newey–West h.a.c. standard error in brackets.

Abbreviations: BK, Barunik and Krehlik; DY, Diebold and Yilmaz; TII, Total Input Intensity; TOI, Total Output Intensity; VAR, vector autoregressive.

*, **, and *** indicate 10%, 5%, and 1% statistical significance levels, respectively.

TABLE B2 | The Fama–MacBeth regression about the future contract with other network factors.

	(1)	(2)	(3)	(4)	(5)	(6)	(7)	(8)
Panel A: The scroll window size is 125, and the predicted step size is 12								
γ_0	0.0004	0.0004	0.0003	0.0004	0.0004	0.0004		
	(0.0009)	(0.0010)	(0.0010)	(0.0010)	(0.0010)	(0.0010)		
$\gamma_{\text{TOI}}^{\text{spr}}$	−0.0011		0.0007		−0.0006			
	(0.0008)		(0.0013)		(0.0014)			
$\gamma_{\text{TII}}^{\text{spr}}$		0.0005		−0.0009		0.0002		
		(0.0013)		(0.0016)		(0.0019)		
$\gamma_{\text{B,High 4}}^{\text{spr}}$	−0.0014	−0.0012	−0.0010	−0.0006	−0.0012	−0.0004		
	(0.0010)	(0.0010)	(0.0011)	(0.0010)	(0.0009)	(0.0016)		
$\gamma_{\text{B,Low 4}}^{\text{spr}}$	−0.0007	−0.0014	−0.0003	−0.0014	−0.0008	−0.0023		
	(0.0020)	(0.0016)	(0.0020)	(0.0023)	(0.0017)	(0.0021)		
$\gamma_{\text{B}}^{\text{nb}}$	−0.0018	0.0008	−0.0005	−0.0011	0.0005	0.0011		
	(0.0025)	(0.0035)	(0.0032)	(0.0022)	(0.0031)	(0.0025)		
Adjusted R^2	0.1499	0.1507	0.1408	0.1413	0.1484	0.1400		
Observations	9324	9324	9324	9324	9324	9324		
Panel B: The scroll window size is 250, and the predicted step size is 20								
γ_0	0.0004	0.0003	0.0004	0.0004	0.0004	0.0004	0.0004	0.0005
	(0.0010)	(0.0010)	(0.0010)	(0.0010)	(0.0010)	(0.0010)	(0.0010)	(0.0010)
$\gamma_{\text{TOI}}^{\text{spr}}$	0.0002		−0.0005		0.0016		0.0023*	
	(0.0013)	(0.0014)		(0.0010)		(0.0013)		
$\gamma_{\text{TII}}^{\text{spr}}$		0.0016		−0.0003		0.0006		−0.0010
		(0.0010)		(0.0011)		(0.0008)		(0.0010)
$\gamma_{\text{B,High 4}}^{\text{spr}}$	−0.0012	−0.0008	−0.0014	−0.0009	−0.0008	−0.0007	−0.0002	−0.0010
	(0.0010)	(0.0013)	(0.0009)	(0.0009)	(0.0012)	(0.0014)	(0.0009)	(0.0011)
$\gamma_{\text{B,Low 4}}^{\text{spr}}$	−0.0008	−0.0018	−0.0009	−0.0010	−0.0021	−0.0017	−0.0009	−0.0015
	(0.0019)	(0.0023)	(0.0018)	(0.0020)	(0.0019)	(0.0023)	(0.0018)	(0.0022)
$\gamma_{\text{B}}^{\text{nb}}$	−0.0003	0.0024	−0.0001	−0.0011	0.0027	0.0013	−0.0004	−0.0000
	(0.0025)	(0.0032)	(0.0035)	(0.0023)	(0.0028)	(0.0027)	(0.0025)	(0.0018)
Adjusted R^2	0.1482	0.1436	0.1294	0.1338	0.1442	0.1357	0.1383	0.1521
Observations	9324	9324	9324	9324	9324	9324	9324	9324

Note: This table presents cross-sectional asset pricing tests for difference factor models for each future contract. We use a sliding window to calculate the beta value of each factor, and use a 1-year window length to calculate the weekly beta of each contract. (1) and (2) are the TOI and TII calculated using the DY framework. (3) and (4) are the short-term TOI and TII calculated using the BK framework. (5) and (6) are the long-term TOI and TII calculated using the BK framework. (7) and (8) are the TOI and TII calculated using the TVP-VAR-based DY framework. We report on the Newey–West h.a.c. standard error in brackets.
Abbreviations: BK, Barunik and Krehlik; DY, Diebold and Yilmaz; TII, Total Input Intensity; TOI, Total Output Intensity.
*, **, and *** indicate 10%, 5%, and 1% statistical significance levels, respectively.